# Theory of tunneling anomalies in superconductors above the paramagnetic limit

Hae-Young Kee
*Serin Physics Laboratory, Rutgers University, Piscataway, New Jersey 08855*

I. L. Aleiner
*NEC Research Institute, 4 Independence Way, Princeton, New Jersey 08540*
*and Department of Physics and Astronomy, SUNY at Stony Brook, Stony Brook, New York 11794*

B. L. Altshuler
*NEC Research Institute, 4 Independence Way, Princeton, New Jersey 08540*
*and Physics Department, Princeton University, Princeton, New Jersey 08544*
(Received 17 February 1998)

We study the tunneling density of states (DOS) in superconducting systems driven by a Zeeman splitting $E_Z$ into the paramagnetic phase. We show that, even though the BCS gap disappears, superconducting fluctuations cause a strong DOS singularity in the vicinity of energies $-E^*$ for electrons polarized along the magnetic field and $E^*$ for the opposite polarization. The position of this singularity $E^*=\frac{1}{2}(E_Z+\sqrt{E_Z^2-\Delta^2})$ (where $\Delta$ is BCS gap at $E_Z=0$) is universal. We found analytically the shape of the DOS for different dimensionalities of the system. For ultrasmall grains the singularity has the shape of a hard gap, while in higher dimensions it appears as a significant though finite dip. Spin-orbit scattering, and an orbital magnetic field suppress the singularity. Our results are qualitatively consistent with recent experiments in superconducting films.
[S0163-1829(98)05529-5]

## I. INTRODUCTION

It is well known that a magnetic field $H$ suppresses superconductivity since it lifts time reversal symmetry (see, e.g., Ref. 1 for a general introduction). In the absence of spin-orbit coupling, this effect can be separated into two mechanisms: (i) the effect of the magnetic field on the orbital motion associated with an Aharonov-Bohm phase, and (ii) the Zeeman splitting of the states with the same spatial wave functions but opposite spin directions.

In bulk systems, the suppression of superconductivity is typically associated with the first mechanism. Indeed, the estimate for the critical field $H_{c_2}$ in this case is

$$H_{c_2}\xi^2 \simeq \phi_0, \tag{1.1}$$

where $\phi_0=hc/2e$ is the superconducting flux quantum and

$$\xi=\sqrt{\frac{D}{\Delta}} \tag{1.2}$$

is the coherence length for the dirty superconductors, $\Delta$ is the BCS gap, and $D$ is the diffusion coefficient. On the other hand, the magnetic field necessary to affect superconductivity by virtue of the spin mechanism is given by

$$g_L\mu_B H_{\rm spin} \simeq \Delta, \tag{1.3}$$

where $g_L$ is the Landé $g$ factor, and $\mu_B=e\hbar/2mc$ is the Bohr magneton. Comparing Eqs. (1.1) and (1.3), one finds that $H_{\rm spin}$ is far in excess of $H_{c_2}$:

$$\frac{H_{\rm spin}}{H_{c_2}} \simeq \epsilon_F\tau \gg 1, \tag{1.4}$$

where $\epsilon_F$ is the Fermi energy and $\tau$ is the elastic momentum relaxation time. Condition (1.4) means that in bulk systems, the orbital effect of the magnetic field is always dominant.

The situation may change in restricted geometries. Consider, e.g., a superconducting film of thickness $a \ll \xi$, placed in a magnetic field parallel to the plane of the film. A Cooper pair in this case is restricted in the transverse direction by the film thickness $a$. As a result, the geometrical area swept by this pair can be estimated as $a\xi$ rather than as $\xi^2$. Therefore, Eq. (1.1) should be changed to

$$H^{\parallel}_{c_2}\xi a \simeq \phi_0 \Rightarrow H^{\parallel}_{c_2} \simeq H_{c_2}\left(\frac{\xi}{a}\right). \tag{1.5}$$

On the other hand, the Zeeman splitting $E_Z=g_L\mu_B H$ is not affected by geometrical restrictions. Accordingly, instead of Eq. (1.4) the ratio of the two scales of magnetic field is given by

$$\frac{H_{\rm spin}}{H^{\parallel}_{c_2}} \simeq (\epsilon_F\tau)\left(\frac{a}{\xi}\right). \tag{1.6}$$

Thus, for sufficiently thin films, $a \ll \xi/\epsilon_F\tau$, the spin effects become dominant. One can easily check that the same estimate (1.6) holds for other restricted systems, i.e., superconducting grains or wires. In these cases, $a$ is the size of the grain or the diameter of the wire, respectively. Quite generally, $a$ is determined by the minimal size of the sample in the plane perpendicular to the magnetic field. In this paper we

 

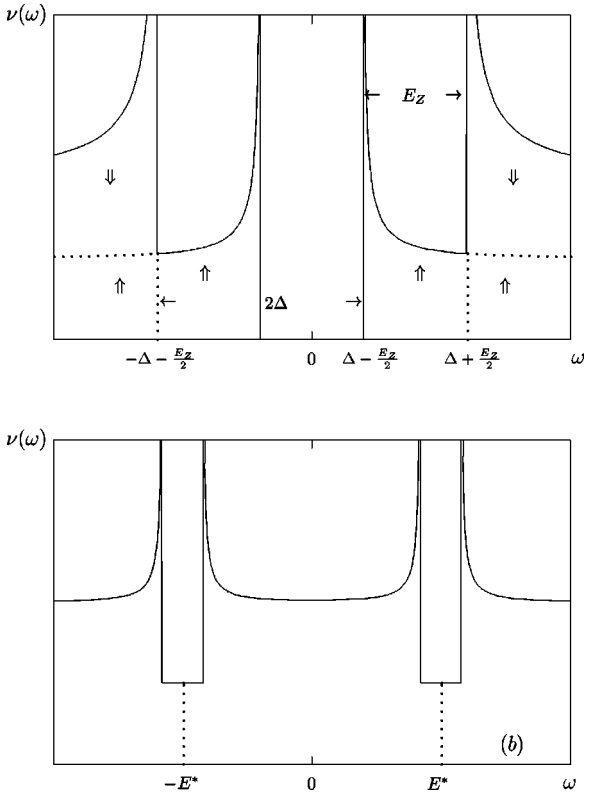


FIG. 1. Evolution of the tunneling DOS with the Zeeman splitting $E_Z$ for (a) the superconducting state, $E_Z<\sqrt{2}\Delta$, see, e.g., Ref. 5, and (b) for the paramagnetic state $E_Z>\sqrt{2}\Delta$. The usual zero-bias anomaly in the paramagnetic state (b) is not shown for simplicity. The shape of the singularity at $E^*$ corresponds to the zero-dimensional case.

consider such restricted geometries, and unless the opposite is stated, neglect orbital effects.

The transition from superconductor to paramagnet is of the first order:[2] the superconducting state is the only stable state at $E_Z\leqslant\Delta$; while at $E_Z\geqslant 2\Delta$ normal state is the only stable state. Both phases are locally stable (i.e., stable with respect to small perturbations) in the interval of magnetic fields where $\Delta<E_Z<2\Delta$. The normal state becomes lowest in energy and thus globally stable at $E_Z\geqslant\sqrt{2}\Delta$. From now on, we will assume that this condition is fulfilled.

One of the most fundamental manifestations of superconductivity is the gap in the tunneling density of states (DOS) around zero bias.[1,3] One can expect that after the paramagnetic transition not only the BCS order parameter vanishes but also the energy dependence of the tunneling DOS becomes similar to those in superconductors above the critical temperature $T_c$. (The latter dependence is discussed in the review article Ref. 4.)

In this paper, we demonstrate that, on the contrary, there are clear observable superconducting effects in the normal state even far from the transition region. We will show that at the transition point there appears a dip in the DOS (a schematic evolution of the DOS with the magnetic field is shown in Fig. 1).

The shape and the width of this dip depend on dimensionality of the system. However, its position is remarkably universal:

$$E^*=\frac{1}{2}(E_Z+\sqrt{E_Z^2-\Delta^2}), \tag{1.7}$$

for the zero-dimensional (0D) (grain), 1D (strip), and 2D (film) cases. Some of our conclusions already have been briefly reported by two of us.[6] Here we present detailed derivations of the results of Ref. 6 and consider the relevant perturbations (spin-orbital coupling, orbital magnetic field, finite temperature, and energy relaxation) of the new tunneling anomaly.

The remainder of the paper is organized as follows. Section II presents the parametrically exact solution for the simplest but instructive geometry of zero-dimensional systems (ultra-small superconducting grains). Section III deals with the more involved problem of the tunneling anomaly in superconducting films and wires. Both sections required application of the diagrammatic technique on the level of at least Ref. 7. For the benefit of the readers interested in physical interpretation rather than in rigorous derivations, we present in Sec. IV the qualitative derivation which grasps all the essential physics involved, even though it fails to give a completely quantitative description. Section V analyzes how the tunneling anomaly is affected by spin-orbital coupling, orbital magnetic field, finite temperature, and energy relaxation. We discuss the recent experiment[8] on the Zeeman splitting of the tunneling anomaly in Al films in Sec. VI. Our findings are summarized in the Conclusion.

## II. ZERO-DIMENSIONAL SYSTEMS

Let us consider an isolated disordered superconducting grain which is small so that the Zeeman splitting dominates over the orbital magnetic field effect (see, e.g, Refs. 9, 10 for recent experiments on such grains). We assume that the size of the grain exceeds the electronic mean free path $l$, and, at the same time, is much smaller than the superconducting coherence length $\xi$. We also assume that $k_F l\gg 1$. This results in a large dimensionless conductance of the grain $g$ $(g\sim k_F^2 l a)$. Finally, we assume that the grain is already driven into the paramagnetic state by the Zeeman splitting. Our goal is to find effects of the superconducting fluctuations on the DOS of the system.

The Hamiltonian $H$ of the system consists of a noninteracting part $H_0$ and an interacting one $H_{\rm int}$. Using the basis of the exact eigenstates of $H_0$ labeled by integers $i$ and $j$, one can write the Hamiltonian as

$$H=\sum_{i\sigma} E_{i\sigma}a_{i\sigma}^{\dagger}a_{i\sigma}-\lambda\overline{\delta}\sum_{i,j} a_{i\uparrow}^{\dagger}a_{i\downarrow}^{\dagger}a_{j\downarrow}a_{j\uparrow}. \tag{2.1}$$

Here the operator $a_{i\sigma}^{\dagger}(a_{i\sigma})$ creates (annihilates) an electron in a state $i$ with spin $\sigma=\uparrow,\downarrow$, and energy $E_{i\uparrow(\downarrow)}=\epsilon_i\mp E_Z/2$ where $\epsilon_i$ is the orbital energy of the $i$th state. $\lambda\ll 1$ is the dimensionless interaction constant, and $\overline{\delta}$ is the average level spacing:

$$\langle\epsilon_{i+1}-\epsilon_i\rangle=\overline{\delta}. \tag{2.2}$$

Let us stop for a moment to discuss the approximation made in Eq. (2.1). We included in Eq. (2.1) only the matrix elements of the interaction Hamiltonian responsible for the

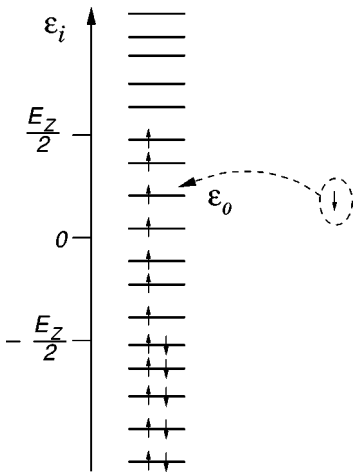


FIG. 2. Structure of the ground state of the superconductor above paramagnetic limit. Electron tunneling onto the orbital $\epsilon_0$, creates a spin singlet state on this orbital. At some energy $\epsilon_0$ mixing of this singlet with the empty states becomes resonant, see the text.

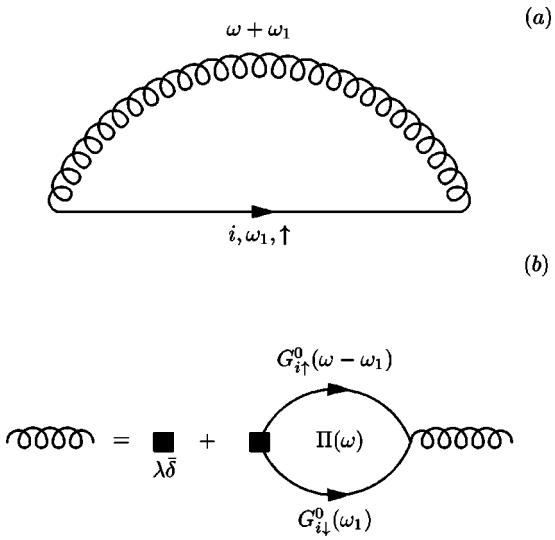


FIG. 3. Diagrams for (a) self-energy $\Sigma_{i,\downarrow}(\omega)$ and (b) superconducting propagator $\Lambda(\omega)$.

superconductivity. We omitted two kinds of diagonal terms. The term proportional to $a^\dagger_{i\sigma_1}a_{i\sigma_1}a^\dagger_{j\sigma_2}a_{j\sigma_2}$ represents the total charging energy responsible for the Coulomb blockade.[11] It is not important for us because it does not lead to any anomalies at energies of the order of Zeeman splitting, and it can be accounted for by a corresponding shift of the applied bias. Other diagonal terms such as the one proportional to $a^\dagger_{i\sigma_1}a_{i\sigma_2}a^\dagger_{j\sigma_2}a_{j\sigma_1}$ represent the spin exchange. It is not included because it leads only to a renormalization of the Landé factor $g_L$.

We also omitted off-diagonal terms, such as $a^\dagger_{i\uparrow}a^\dagger_{j\downarrow}a_{k\downarrow}a_{l\uparrow}$ with $i, j, k, l$ not equal pairwise, corresponding to the matrix elements:

$$M^{kl}_{ij}=\int dr dr' V(r-r')\psi^*_i(r)\psi^*_j(r')\psi_k(r)\psi_l(r').$$

The wave functions are known to oscillate very fast, so the wave functions of different levels are very weakly correlated. We can restrict our consideration by a short-range interaction, $V(r-r')=(\lambda/\nu_0)\,\delta(r-r')$, where $\nu_0$ is the bare DOS. One sees that the integrand $[|\psi_i(r)|^2|\psi_j(r)|^2]$ in the diagonal matrix elements is always positive while the product $[\psi^*_i(r)\psi^*_j(r)\psi_k(r)\psi_l(r)]$ can be both positive and negative. As a result, the off-diagonal matrix elements turn out to be smaller than diagonal ones. Straightforward calculations[12,13] show that they are smaller by a factor $1/g$.

In the paramagnetic state ($E_Z>\sqrt{2}\Delta$), the structure of the ground state is similar to that without interaction, see Fig. 2. The orbitals with $\epsilon_i<-E_Z/2$ are doubly occupied while those with $\epsilon_i>E_Z/2$ are empty. The orbitals with $|\epsilon_i|<E_Z/2$ are spin polarized with spin up.

The Hamiltonian (2.1) does not affect the spin polarized states, but mixes the doubly occupied and empty states. Since those states are separated from each other by a large gap $E_Z$, this mixing can be treated perturbatively. Thus, the mixing does not change the ground state qualitatively. In contrast, the spectrum of the excitations, i.e., the tunneling DOS changes drastically due to the interaction. The essence of this effect is that a spin-down electron tunneling into some orbital $\epsilon_0$ already occupied by a spin-up electron creates an electron pair which can mix with the empty orbitals and thus interact with superconducting fluctuations. This mixing turns out to be resonant at some energy $E=E^*$ and it leads to a sharp singularity in the spectrum of one-electron excitation.

To evaluate the effect of superconducting fluctuations on the DOS of electrons in the paramagnetic state, we use the diagrammatic technique for the Green function (GF) at zero temperature.[7] The DOS can be expressed through the one-particle GF, $G_{i\sigma}(\omega)$, of an electron on the orbital $j$ and with spin $\sigma=\pm1\equiv\uparrow(\downarrow)$:

$$\nu_\sigma(\omega)=-\frac{1}{\pi}\,\mathrm{sgn}(\omega)\mathrm{Im}\sum_i G_{i\sigma}(\omega), \tag{2.3}$$

where

$$G^{-1}_{i\sigma}=G^{0-1}_{i\sigma}-\Sigma_{i\sigma}. \tag{2.4}$$

$G^0_{i\sigma}$ is the GF for the noninteracting system

$$G^0_{i\uparrow(\downarrow)}=(\omega_+-\epsilon_i\pm E_Z/2)^{-1}, \tag{2.5}$$

and $\Sigma_{i\sigma}$ is the one particle self-energy.

The leading contribution to the self-energy is shown in Fig. 3(a). The solid and curly lines denote the single-particle GF and the propagator of superconducting fluctuations, respectively. The latter can be obtained by summing the polarization loops in the Cooper channel shown in Fig. 3(b). The single loop is given by

$$\Pi(\omega)=\frac{1}{2\bar{\delta}}\ln\left(\frac{\omega_c^2}{E_Z^2-\omega_+^2}\right), \tag{2.6}$$

where $\omega_+=\omega+i0\,\mathrm{sgn}(\omega)$ and $\omega_c$ is the high-energy cutoff. Solving the Dyson equation [Fig. 3(b)], we obtain the propagator

$$\Lambda(\omega)=\frac{\lambda\bar{\delta}}{1-\lambda\bar{\delta}\Pi(\omega)}=\frac{2\bar{\delta}}{\ln[(E_Z^2-\omega_+^2)/\Delta^2]}, \tag{2.7}$$

where $\Delta=\omega_c\exp(-1/\lambda)$ is the BCS gap.

The propagator (2.7) has a pole at $\omega=\pm\Omega$,

$$\Omega=\sqrt{E_Z^2-\Delta^2}. \tag{2.8}$$

This pole can be interpreted as a bound state of two quasiparticles with energy $\Omega$.

The analytic expression for the self-energy given by Fig. 3(a), has the form

$$\Sigma_{i\downarrow}(\omega)=i\int_{-\infty}^{\infty}\frac{d\omega_1}{2\pi}\Lambda(\omega+\omega_1)G^0_{i\uparrow}(\omega_1). \tag{2.9}$$

One can see that there are two contributions to the self-energy. One comes from the pole of $\Lambda$ and the other is due to the branch cut of this propagator. The pole contribution gives a singularity of the self-energy at certain $\omega$ and $\epsilon_i$ while the contribution of the branch cut is smooth. To find the singularity in the DOS, only the pole contribution to $\Sigma$ may be retained:

$$\Sigma_{i\downarrow}(\omega)=\frac{\overline{\delta}\Delta^2}{\Omega}\,\frac{1}{\omega_+ +\epsilon_i-E_Z/2+\Omega\ \mathrm{sgn}(\epsilon_i-E_Z/2)}. \tag{2.10}$$

At certain $\omega$ the pole of the self-energy coincides with the pole of $G^0$. This causes the singularity in the DOS. One can check that the singularities of Eqs. (2.5) and (2.10) coincide provided $\epsilon_i=\Omega/2$ and

$$\omega=\frac{E_Z+\Omega}{2}=\frac{E_Z+\sqrt{E_Z^2-\Delta^2}}{2}\equiv E^*. \tag{2.11}$$

Substituting Eq. (2.10) into Eq. (2.4) we obtain the GF for the down-spin electron at $\omega$ close to $E^*$:

$$G_{i\downarrow}(\omega)=\frac{\omega_+ +\epsilon_i-E_Z/2-\Omega}{(\omega_+ -\epsilon_i-E_Z/2)(\omega_+ +\epsilon_i-E_Z/2-\Omega)-W_0^2}, \tag{2.12}$$

where the energy scale of the singularity is given by

$$W_0=\sqrt{\frac{\overline{\delta}\Delta^2}{\Omega}}. \tag{2.13}$$

Since $E_Z,\Delta\gg\overline{\delta}$, one can neglect the fine structure of the DOS on the scale of $\overline{\delta}$ and substitute the summation over $i$ by the integration over $\epsilon_i$:

$$\sum_i G_{i\downarrow}=\nu_0\int d\epsilon_i\frac{\omega_+ +\epsilon_i-E_Z/2-\Omega/2}{-\epsilon_i^2+(\omega_+ -E_Z/2-\Omega/2)-W_0^2}$$

$$=-i\nu_0\pi\frac{\omega-E^*}{\sqrt{(\omega-E^*)^2-W_0^2}}. \tag{2.14}$$

Analogously, the GF for the up-spin electron can be obtained by changing the signs of $E_Z$ and $\Omega$, so that the singularity occurs at $\omega=-E^*$.

Substituting Eq. (2.14) into Eq. (2.3), we obtain the final expression for the tunneling DOS in ultrasmall grains

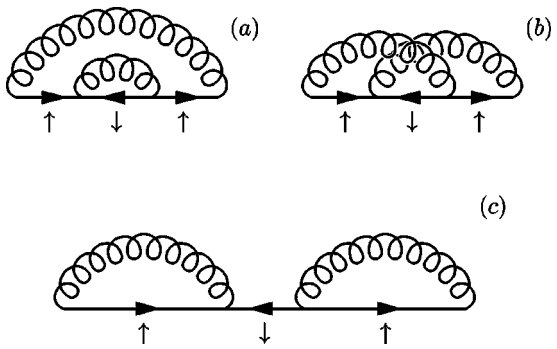


FIG. 4. Higher-order corrections to the self-energy (a) and (b), which were neglected in comparison with reducible diagram (c).

$$\nu_{\uparrow(\downarrow)}(\omega)=\nu_0F_0\left(\frac{\omega\pm E^*}{W_0}\right),\quad F_0(x)=\mathrm{Re}\left(\frac{x^2}{x^2-1}\right)^{1/2}, \tag{2.15}$$

where $\nu_0$ is the bare DOS per one spin, the energy $E^*$ is defined by Eq. (1.7) and the width of the singularity $W_0$ is given by Eq. (2.13). Equations (2.15) and (2.13) are the main result of this section. They predict a hard gap in the spin-resolved density of states: $\nu_\sigma(\omega)$ vanishes at $|\omega+\sigma E^*|<W_0$. The overall density of states $\nu_\downarrow+\nu_\uparrow$ is suppressed by a factor of 2 near the singularity.

In this calculation we neglected higher corrections to the self-energy, e.g., those shown in Figs. 4(a) and 4(b). In order to justify this approximation, we have to compare the contributions shown in Figs. 4(a) and 4(b) with the reducible diagram shown in Fig. 4(c) included in Eqs. (2.10) and (2.12). The singular contribution originates from the pole of $\Lambda$. It means that $\Lambda$ carries frequency $\Omega$. The singularity in the DOS at $\omega=E^*$ appears when the pole of the self-energy and the pole of $G^0$ coincide. This happens when the GF $G^0$ for up-spin carries energy $\Omega-\omega$. In Figs. 4(a)–4(c), the intermediate $G^0$ for down-spin should carry energy $\omega$ to give a singularity to the DOS at $E^*$. This condition cannot be satisfied for Figs. 4(a) and 4(b). As a result, after the integration over the intermediate frequency, these higher-order corrections turn out to be smaller than the reducible contribution (c) by small factor $W_0/\Delta\simeq\sqrt{\overline{\delta}/\Delta}\ll 1$.

## III. DISORDERED INFINITE SYSTEMS

In this section, we will obtain quantitative results for the tunneling anomaly in infinite systems. In Sec. III A we will start from the perturbation theory and demonstrate that the lowest order perturbative results diverge algebraically at energies close to $E^*$. In order to deal with this divergence, we develop a nonperturbative approach in Sec. III B and obtain the analytic expressions for the shape of the singularities for all interesting cases. This machinery will be also used later in Sec. V.

### A. Perturbative results

The analysis of a 0D system presented in the previous subsection, is not directly applicable to superconducting wires and films because one cannot approximate the interaction Hamiltonian

$$\hat{H}_{\rm int}=-\lambda\nu_0^{-1}\int_{-\infty}^{\infty}dr a_\uparrow^\dagger(r)a_\downarrow^\dagger(r)a_\downarrow(r)a_\uparrow(r) \qquad (3.1)$$

by its diagonal matrix elements. Despite this complication, we will still be able to show that the singularity persists and remains at the same bias as that in 0D.

To describe this singularity we once again have to evaluate the effect of the superconducting fluctuations on the GF of electrons. First of all, we need to evaluate the propagator of superconducting fluctuations $\Lambda$, see Fig. 5. In contrast with the 0D case, the superconducting fluctuations in the bulk system are inhomogeneous: the propagator for the superconducting fluctuations depends on the wave vector $Q$. (We will omit the vector notation in the momenta, e.g., $Q\equiv\vec{Q}$.) Solving the Dyson equation shown in Fig. 5(a), we obtain the propagator

$$\Lambda(\omega,Q)=\frac{2}{\nu_0\ln\{[E_Z^2-(|\omega|+iDQ^2)^2]/\Delta^2\}}, \qquad (3.2)$$

where $D$ is the diffusion coefficient. At $Q=0$, the propagator (3.2) resembles the zero-dimensional expression (2.7). We see that the propagator has a singularity at $\omega$ close to $\Omega$ provided $DQ^2\ll\Omega$. As we will see shortly, it results in the singularity in the DOS developing at exactly the same energy as in the 0D case, $\omega=E^*$, given by Eq. (2.11).

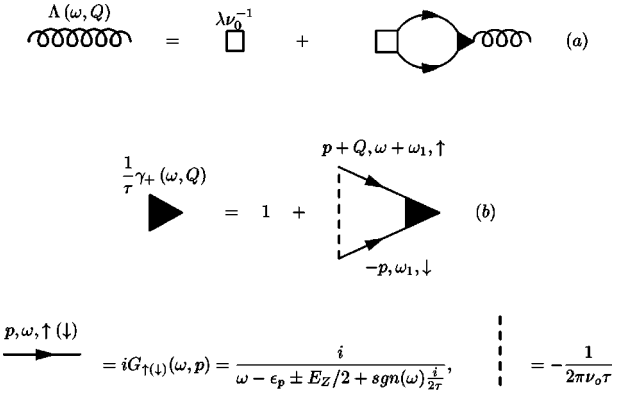


FIG. 5. Diagrams for the (a) propagator of superconducting fluctuations $\Lambda(\omega,Q)$ and (b) the vertex function $\gamma_+(\omega,Q)$.

The next step is to consider the vertex function in the particle-particle channel. The ladder approximation which gives the main contribution at $\epsilon_F\tau\gg1$ ($\tau$ is the elastic mean free time) is shown in Fig. 5(b). Analytically, they are given by

$$\gamma_\pm(\omega,Q)=\tau+I_\pm(\omega,Q)\gamma_\pm(\omega,Q). \qquad (3.3)$$

Here $I_\pm(\omega,Q)$ stands for

$$\begin{aligned}I_\pm(\omega,Q)&=\frac{1}{2\pi\nu_0\tau}\int(dp)G_{\uparrow(\downarrow)}(\omega+\omega_1,\epsilon_p)G_{\downarrow(\uparrow)}(\omega_1,\epsilon_{-p-Q})\\&=\frac{1}{2\pi\nu_0\tau}\int(dp)\frac{1}{[\omega+\omega_1-\epsilon_p\pm E_Z/2+(i/2\tau)\,\mathrm{sgn}(\omega+\omega_1)][\omega_1-\epsilon_{-p+Q}\mp E_Z/2+(i/2\tau)\,\mathrm{sgn}(\omega_1)]}\\&=\{1+\tau[i(|\omega|\pm\mathrm{sgn}(\omega)E_Z)-DQ^2]\}\theta[-(\omega+\omega_1)\omega],\end{aligned} \qquad (3.4)$$

where $(dp)=d^dp/(2\pi)^d$, and the GF's are averaged over disorder.[7,4] Here we used the conditions of the diffusion approximation, $\omega\tau\ll1$ and $Ql\ll1$. We substitute Eq. (3.4) into Eq. (3.3) and we obtain

$$\gamma_\pm(\omega,Q)=\tau\theta[(\omega+\omega_1)\omega]+\frac{\theta[-(\omega+\omega_1)\omega]}{-i[|\omega|\pm\mathrm{sgn}(\omega)E_Z]+DQ^2}. \qquad (3.5)$$

Now we can evaluate the first-order correction to the one-particle GF, Fig. 6:

$$\delta G_\downarrow^{(1)}(\omega,p)=\frac{1}{\tau^2}\int(dQ)\int\frac{d\omega_1}{2\pi}G_\downarrow^2(\omega,p)\Lambda(\omega+\omega_1,Q)\times G_\uparrow(\omega_1,-p+Q)\gamma_-^2(\omega-\omega_1,Q). \qquad (3.6)$$

The DOS is determined by the GF integrated over $p$:

$$\nu_{\uparrow(\downarrow)}(\omega)=-\frac{\mathrm{sgn}(\omega)}{\pi}\,\mathrm{Im}\int(dp)G_{\uparrow(\downarrow)}(\omega,p). \qquad (3.7)$$

We substitute Eq. (3.5) into Eq. (3.7) and perform the integration over $p$ and $\omega_1$. For $Ql\ll1$ and $|\omega-\omega_1|\tau\ll1$ integration over the momentum $p$ results in

$$\int(dp)G_\downarrow^2(\omega,p)G_\uparrow(\omega_1,-p+Q)=i2\pi\nu_0\theta(-\omega\omega_1)\tau^2\mathrm{sgn}(\omega_1).$$

Performing the integration over $\omega_1$ we take into account only the pole contributions in the propagator (3.2) for $DQ^2\ll\Omega$:

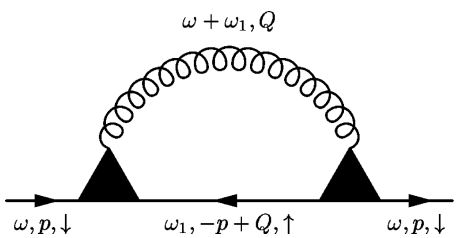


FIG. 6. Diagrams for the lowest order corrections to the one-particle Green function.

$$\Lambda(\omega,Q)\approx\frac{\Delta^2}{\nu_0\Omega}\left(\frac{1}{\Omega+\omega-iDQ^2}+\frac{1}{\Omega-\omega-iDQ^2}\right), \tag{3.8}$$

since the integrals along the branch cuts give only the corrections which are smooth functions of $\omega$. The main contribution to the frequency integral results from the region where the real part of the pole of the propagator $\Lambda$ in Eq. (3.7), Re $\omega_1=-\omega\pm\Omega$, is close to that of the vertex $\gamma_-$, Re $\omega_1=\omega+\mathrm{sgn}(\omega_1-\omega)E_Z$, and the imaginary parts of those poles have different signs. The latter requires $\omega$ Re $\omega_1<0$, $\omega^2>[\mathrm{Re}\ \omega_1]^2$. One can easily check that all these conditions can be met only if $\omega$ is close to $E^*$ from Eq. (1.7).

Evaluating the integral over $\omega_1$ in Eq. (3.7) we obtain the first-order correction to the DOS

$$\frac{\delta\nu^{(1)}_{\uparrow(\downarrow)}(\omega)}{\nu_0}=-\frac{\Delta^2}{2\nu_0\Omega}\,\mathrm{Re}\int(dQ)C^2_{\uparrow(\downarrow)}(\omega,Q), \tag{3.9}$$

where $C_{\uparrow(\downarrow)}(\omega,Q)$ is the Cooperon given by

$$C_{\uparrow(\downarrow)}(\omega,Q)=\frac{1}{-i|\omega\pm E^*|+DQ^2}. \tag{3.10}$$

[Calculation of $\delta\nu_\uparrow$ requires an obvious modification of Eq. (3.7).]

For the one-dimensional case (wire), this correction acquires the form

$$\frac{\delta\nu^{(1)}_{\uparrow(\downarrow)}}{\nu_0}(\omega)=\frac{\sqrt{\Delta}}{8\nu_0\Omega\sqrt{2D}}\left(\frac{\Delta}{|\omega\pm E^*|}\right)^{3/2}. \tag{3.11}$$

It is possible to neglect higher-order corrections to the DOS only provided $|\omega\pm E^*|$ is large. For $\omega\to E^*$, the correction (3.11) diverges. Therefore we need to sum up all the orders of perturbation theory to describe the DOS in the vicinity of $E^*$. Such a calculation is carried out in the next subsection.

For two dimensions (films), the first-order correction to the DOS vanishes for $|\omega|\neq E^*$. However, this is nothing but an artifact of the first-order approximation and the second-order correction is already finite. Diagrams for this correction are shown in Fig. 7. The result can be written as

$$\frac{\delta\nu^{(2)}_{\uparrow(\downarrow)}(\omega)}{\nu_0}=-2\left(\frac{\Delta^2}{4\nu_0\Omega}\right)^2\frac{\partial}{\partial\omega}\,\mathrm{Im}\int(dQ_1)(dQ_2)\times C^2_{\uparrow(\downarrow)}(\omega,Q_1)C_{\uparrow(\downarrow)}(\omega,Q_2). \tag{3.12}$$

For the two-dimensional case Eq. (3.12) gives

$$\frac{\delta\nu^{(2)(\omega)}_{\uparrow(\downarrow)}}{\nu_0}=-\left[\frac{\Delta^2}{4g\Omega(\omega\pm E^*)}\right]^2\ln\left(\frac{\Omega}{|\omega\pm E^*|}\right)^2, \tag{3.13}$$

where $g=4\pi D\nu_0\gg1$ is the dimensionless conductance of the film in the normal state. Deriving Eq. (3.13), we cut off the logarithmic divergence at large momenta $Q_2$ by the condition $DQ_2^2\lesssim\Delta$, since it determines the applicability of a single pole approximation (3.8).

As well as the 1D case, the perturbation theory fails to describe the DOS in the vicinity of $E^*$ in two dimensions. It is noteworthy that the singularity described by Eq. (3.13) is much more pronounced than that of the normal metal ($T>T_c$) which arises due to the superconducting fluctuations and is of the order of $g^{-1}\ln[\ln(\omega\pm E_Z)]$, see Ref. 4. The enhancement of this singularity results directly from the isolated pole in the propagator of the superconducting fluctuations, see Eqs. (3.2) and (3.8) rather than in the branch cuts of Ref. 4.

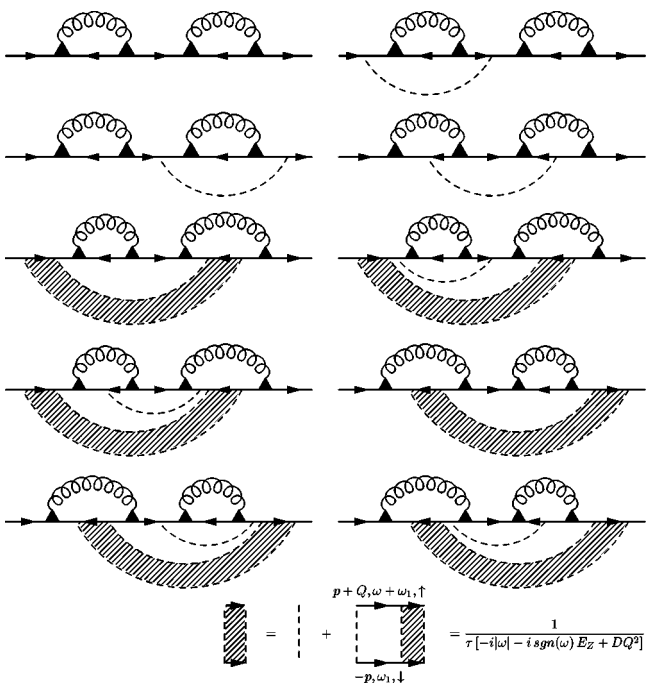


FIG. 7. Diagrams for the second-order corrections to the DOS. Diagrams irreducible with respect to the curly lines, similar to Figs. 4(a) and 4(b), are negligible for the reason discussed in the end of Sec. II.

### B. Nonperturbative results

#### *1. Derivation of self-consistency equations*

We start the summation of the perturbation theory terms from the series of diagrams for the DOS presented in Fig. 8. Such diagrams dominate in each order of the perturbation theory in comparison with those of the same order but in-

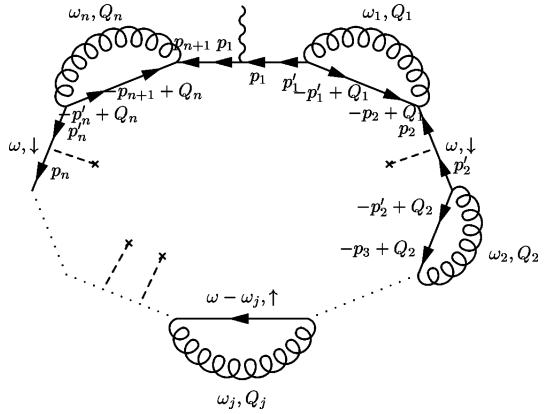


FIG. 8. Structure of the $k$th order perturbation theory. The vertical wiggly line on the upper Green function corresponds to cutting this GF into two lines and fixing its frequency $\omega$.

cluding elements irreducible with respect to curly lines, similar to Figs. 4(a) and 4(b). The latter statement can be justified by arguments similar to the analysis of Figs. 4 presented in the end of Sec. II.

The diagram of the $k$th order of the perturbation theory, Fig. 8, contains $k$ curly lines that stand for the fluctuation propagator $\Lambda(\omega_j,Q_j)$ in Eq. (3.2) ($1\leqslant j\leqslant k$). It also contains $(2k+1)$ GF. Before averaging over disorder, each GF $G_\sigma(\omega;p,p')$ depends on two momenta (initial $p$ and final $p'$) and on the direction of the spins $\sigma=\pm\equiv\uparrow,\downarrow$. Contribution of this diagram to the DOS of $\downarrow$ electrons $\delta\nu_\downarrow(\omega)$ at positive energy $\omega>0$ is

$$\delta\nu_\downarrow^{(k)}(\omega)=-\frac{\mathrm{sgn}(\omega)}{\pi}\mathrm{Im}\int\frac{d\omega_1 d\omega_2\cdots d\omega_k}{(2\pi)^k}\int(dp_1)(dp_1')\cdots(dp_{k+1})\int(dQ_1)(dQ_2)\cdots(dQ_k)$$
$$\times G_\downarrow(\omega;p_{k+1},p_1)\prod_{j=1}^{k}\Lambda(\omega_j,Q_j)G_\downarrow(\omega;p_j,p_j')G_\uparrow(-\omega+\omega_j;-p_j'+Q_j,-p_{j+1}+Q_j). \tag{3.14}$$

Disorder averaging of the product of the Green functions in Eq. (3.14) and of the superconducting propagator $\Lambda$ can be carried out independently, since their correlation gives rise to nonsingular corrections containing additional smallness $1/(\epsilon_F\tau)$.

For the sake of convenience we introduce $G^{R(A)}(\omega;p,p')$: retarded (advanced) GF at $E_Z=0$. In the absence of spin-orbit scattering the Green functions $G^{R(A)}(\omega;p,p')$ from Eq. (3.14) can be presented through $G^{R(A)}$ as

$$G_\sigma(\omega;p,p')=\begin{cases}G^R(\omega+\sigma E_Z/2;p,p') & \omega>0,\\ G^A(\omega+\sigma E_Z/2;p,p') & \omega<0.\end{cases} \tag{3.15}$$

After substituting Eqs. (3.15) and (3.8) into Eq. (3.14), one can integrate over all intermediate frequencies $\omega_j$, because the fluctuation propagator $\Lambda(\omega_j,Q_j)$ has simple poles at $\omega_j=\pm\Omega\mp iDQ_j^2$. According to Eq. (3.15), $G_\downarrow(\omega;p,p')$ in Eq. (3.14) is retarded ($\omega>0$). In order to get the advanced GF from $G_\uparrow(\omega_j-\omega;-p_j'+Q_j,-p_{j+1}+Q_j)$ we choose the pole in $\Lambda(\omega_j;Q_j)$ with positive real part, $\omega_j=\Omega-iDQ_j^2$. (One can check that another pole leads to a product of the retarded functions, which vanish after the disorder averaging.) Using Eqs. (3.8) and (2.8) and introducing the shorthand notation

$$\omega_{Q_j}\equiv-\omega+2E^*-iDQ_j^2, \tag{3.16}$$

we can present $\delta\nu_\downarrow^{(k)}(\omega)$ at $\omega>0$ as

$$\delta\nu_\downarrow^{(k)}(\omega)=-\frac{1}{\pi}\left(\frac{\Delta^2}{\nu_0\Omega}\right)^k\mathrm{Im}\int(dp_{k+1})G^R(\omega;p_{k+1},p_1)$$
$$\times\prod_{j=1}^{n}(dp_j)(dp_j')(dQ_j)G^R(\omega;p_j,p_j')$$
$$\times G^A(\omega_{Q_j};-p_j'+Q_1,-p_{j+1}+Q_j). \tag{3.17}$$

Averaging Eq. (3.17) over disorder and using the identity

$$\int(dp_1)G^R(\omega;p_1,p_1')G^R(\omega;p_{k+1},p_1)$$
$$=-\frac{\partial}{\partial\omega}G^R(\omega;p_{k+1},p_1'), \tag{3.18}$$

we obtain

$$\langle\delta\nu_\downarrow^{(k)}(\omega)\rangle=-\frac{1}{\pi}\left(\frac{\Delta^2}{\nu_0\Omega}\right)^k\left(\frac{1}{2k}\right)\frac{\partial}{\partial\omega}$$
$$\times\mathrm{Im}\left\langle\int\prod_{j=1}^{k}(dQ_j)(dp_j)(dp_j')G^R(\omega;p_j,p_j')\right.$$
$$\left.\times G^A(\omega_{Q_j};-p_j'+Q_j,-p_{j+1}+Q_j)\right\rangle. \tag{3.19}$$

The role of the factor $1/k$ in Eq. (3.19) is to cancel the multiple counting: there are $k$ retarded GF in Eq. (3.19), and application of the operator $\partial_\omega$ to any one of them leads to Eq. (3.17). In addition, Eq. (3.19) includes terms like $\partial G^A/\partial\omega$. One can check that they give exactly the same contribution

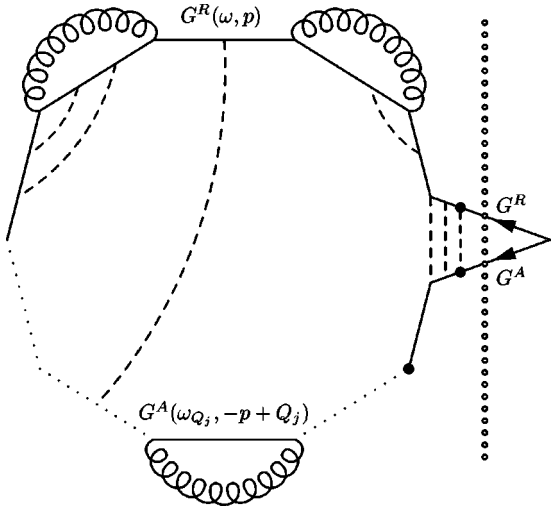


FIG. 9. Structure of $\gamma^{(k)}$. Three points defining the vertex are denoted by thick dots.

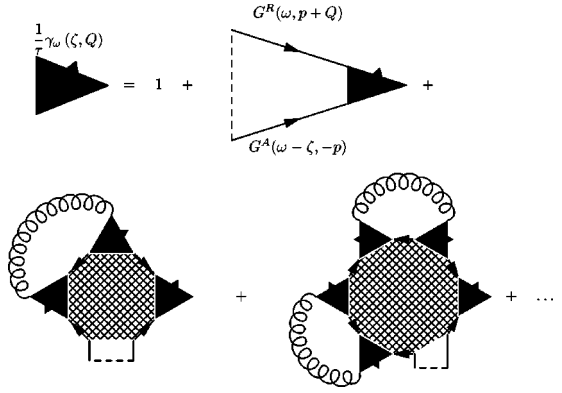


FIG. 10. Diagrammatic equation for the vertex $\gamma_\omega(\zeta,Q)$.

as terms which contain $\partial G^R/\partial\omega$. The additional factor 1/2 takes these contributions into account.

Using a conventional trick $1/k=\int_0^1\eta^k d\eta$, (see Ref. 7), one can present $\langle\delta\nu_\downarrow^{(k)}(\omega)\rangle$ in a form

$$\langle\delta\nu_\downarrow^{(k)}(\omega)\rangle=-\frac{1}{2\pi\tau}\frac{\Delta^2}{\nu_0\Omega}\mathrm{Im}\frac{\partial}{\partial\omega}\int_0^1 d\eta\int(dQ)(dp)\times\langle G^R(\omega;p)\rangle\langle G^A(\omega_Q;-p+Q)\rangle \quad (3.20)$$

where the short-hand notation

$$\tilde{\omega}_Q=\omega-\omega_Q=2\omega-2E^*+iDQ^2 \quad (3.21)$$

is used and $\omega_Q$ is defined in Eq. (3.16). A similar equation holds for spin up and negative $\omega$. In this case one should use $\tilde{\omega}_Q=-2\omega-2E^*+iDQ^2$.

The vertex $\gamma^{(k)}$ can be written using Fig. 9. The rules of reading diagrams on Figs. 9 and 10 are slightly different from the conventional rules we used before: (i) to each curly line corresponds factor $\eta\Delta^2/(\nu_0\Omega)$; (ii) no summation over the frequencies is implied: each retarded GF bears the frequency $\omega$, each advanced GF bears the frequency $\omega_Q$ given by Eq. (3.16); (iii) each interaction with curly lines changes the retarded Green function to advanced and back. The resulting expression reads

$$\gamma_\omega^{(k)}(\tilde{\omega}_Q,Q)=\tau\left(\eta\frac{\Delta^2}{\nu_0\Omega}\right)^{k-1}\left\langle\int\prod_{j=1}^{k-1}(dQ_j)(dp_j)(dp_j')\times G^R(\omega;p_j,p_j')G^A(\omega_{Q_j};-p_j'+Q_j,-p_{j+1}+Q_j)\times G^R(\omega;p_1',p)G^A(\omega_Q;-p_k'+Q,-p+Q)\right\rangle. \quad (3.22)$$

Note that the averaged product of GF's in the integrand of Eq. (3.22) does not depend on $p$. We can thus perform in Eq. (3.20) the integration over $p$. As a result, Eq. (3.22) takes a form

$$\frac{\delta\nu}{\nu_0}=-\frac{\Delta^2}{\nu_0\Omega}\,\mathrm{Im}\frac{\partial}{\partial\omega}\int_0^1 d\eta\int(dQ)\,\gamma(\tilde{\omega}_Q,Q), \quad (3.23)$$

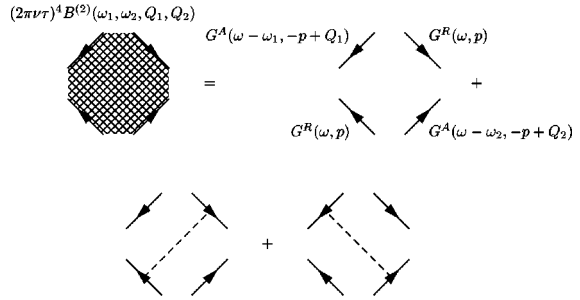


FIG. 11. Second-order Hikami box $B^{(2)}$.

where

$$\gamma(\tilde{\omega}_Q,Q)=\sum_{k=1}^{\infty}\gamma^{(k)}(\tilde{\omega}_Q,Q). \quad (3.24)$$

Our goal is to evaluate $\gamma(\tilde{\omega}_Q,Q)$ self-consistently. The difficulty is that the diagrammatic series for $\gamma$ contains other elements except $\gamma$ itself, see Fig. 10.

These elements are known as Hikami boxes.[14] The simplest Hikami box $B^{(2)}$, which appears already in the second order of the perturbation theory for $\delta\nu$, is the integral $(dp)$ of the sum of the three diagrams shown in Fig. 11

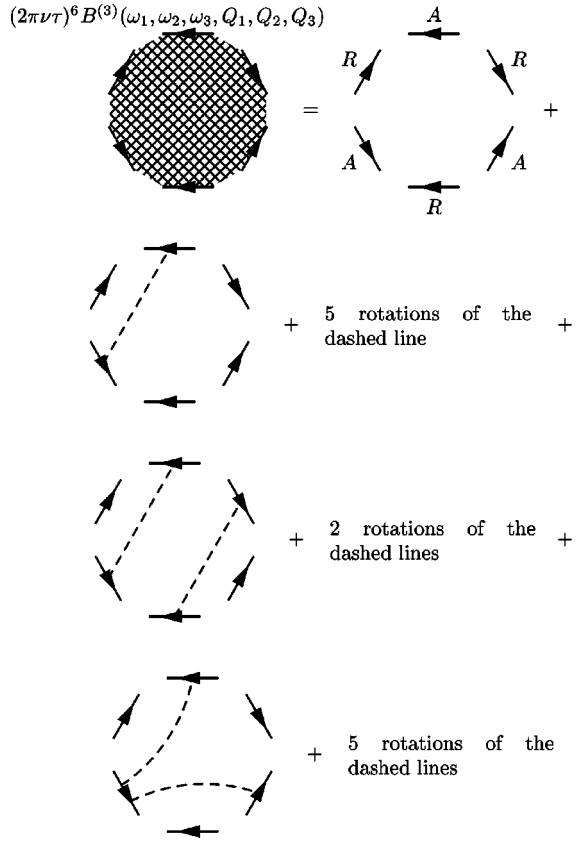


FIG. 12. Third-order Hikami box $B^{(3)}$. Momenta and frequencies in the Green functions are arranged similar to Fig. 11.

$$B^{(2)}(\omega_1,\omega_2,Q_1,Q_2) = \frac{1}{(2\pi\nu_0)^3}[-i(\omega_1+\omega_2)+D(Q_1^2+Q_2^2)]. \tag{3.25}$$

The third-order Hikami box, $B^{(3)}$, is given by the momentum integral $(dp)$ of a sum of 16 diagrams of Fig. 12:

$$B^{(3)}(\omega_1,\omega_2,\omega_3;Q_1,Q_2,Q_3) = -\frac{2}{(2\pi\nu_0)^5}[-i(\omega_1+\omega_2+\omega_3) + D(Q_1^2+Q_2^2+Q_3^2)]. \tag{3.26}$$

The equation for the vertex $\gamma(\tilde{\omega}_Q,Q)\equiv\gamma_\omega(\zeta=\tilde{\omega}_Q,Q)$ that determines the correction to the DOS [Eq. (3.23)] is

$$\frac{1}{\tau}\gamma_\omega(\zeta,Q) = 1+\left(\frac{1}{\tau}+i\zeta-DQ^2\right)\gamma_\omega(\zeta,Q)+\eta\left(\frac{\Delta^2}{\nu_0\Omega}\right)\int (dQ_1)(2\pi\nu_0)^3 B^{(2)}(\tilde{\omega}_Q,\tilde{\omega}_{Q_1},Q,Q_1)\gamma^2(1)\gamma_\omega(\zeta,Q) + \eta^2\left(\frac{\Delta^2}{\nu_0\Omega}\right)^2\int\int (dQ_1)(dQ_2)(2\pi\nu_0)^5 B^{(3)}(\tilde{\omega}_Q,\tilde{\omega}_{Q_1},\tilde{\omega}_{Q_2},Q,Q_1,Q_2)\gamma^2(1)\gamma^2(2)\gamma_\omega(\zeta,Q)+\cdots, \tag{3.27}$$

where $\gamma(j)=\gamma_\omega(\tilde{\omega}_{Q_j},Q_j)$ with $\tilde{\omega}_{Q_j}$ determined by Eq. (3.21). We introduced the extra variable $\zeta$ in order to separate the external energy $\omega$ and the integration variable in Eq. (3.27) and further.

The Hikami box of the $k$th order $B^{(k)}$ is given by a sum of diagrams (of the type of Figs. 11 and 12) which contain $2k$ vertices. Strictly speaking, $B^{(k)}$ depends on $2k-1$ sets of momentum and energy transfer $(\omega,Q)$. However, in order to evaluate the DOS correction given by Fig. 8, we can restrict ourselves by Hikami boxes that depend only on $k$ sets $(\omega_j,Q_j)$, $1\leqslant j\leqslant k$: $(\omega_j,Q_j)$ and $(-\omega_j,-Q_j)$ characterize neighboring vertices. Equations (3.25) and (3.26) allow us to conjecture that $B^{(k)}$ at arbitrary $k$ has a form

$$B^{(k)}\{\omega_j,Q_j\} = \frac{C_k}{(2\pi\nu_0)^{2k-1}}\sum_{j=1}^{k}(-i\omega_j+DQ_j^2), \tag{3.28}$$

where $C_k$ are numerical coefficients.

We are not going to determine coefficients $C_k$ directly. An important feature of Hikami boxes is that they are local objects, determined by distances smaller or of the order of the mean free path $l$. Therefore, the coefficients $C_k$ in Eq. (3.28) do not depend on the dimensionality. Therefore, we can compare the exact solution of the 0D problem, Sec. II, with the sum of the perturbation theory series involving the coefficients $C_k$ and thus find those coefficients.

Equation (3.27) can be rewritten in terms of $C_k$ as

$$(-i\zeta+DQ^2)\gamma_\omega(\zeta,Q) = 1+(-i\zeta+DQ^2)\gamma_\omega(\zeta,Q)\sum_{k=1}^{\infty}C_k\left[\eta\frac{\Delta^2}{\nu_0\Omega}\int(dQ_1)\gamma(1)^2\right]^k+\gamma_\omega(\zeta,Q)\sum_{k=1}^{\infty}kC_k \times\left[\eta\frac{\Delta^2}{\nu_0\Omega}\int(dQ_1)\gamma_\omega(\tilde{\omega}_{Q_1},Q_1)^2\right]^{k-1}\int(dQ_2)(-i\tilde{\omega}_{Q_2}+DQ_2^2)\gamma_\omega(\tilde{\omega}_{Q_2},Q_2)^2. \tag{3.29}$$

Introducing the function $f(x)$,

$$f(x) = -\sum_{k=1}^{\infty}C_kx^k+1, \tag{3.30}$$

we obtain a simple equation for $\gamma_\omega(\zeta,Q)$

$$(-i\zeta+DQ^2)\gamma_\omega(\zeta,Q)f(\beta_0)+\gamma_\omega(\zeta,Q)\beta_1f'(\beta_0)=1, \tag{3.31}$$

where $\beta_0$ and $\beta_1$ are connected with $\gamma$ by

$$\beta_0(\omega) = \eta\frac{\Delta}{\nu_0\Omega}\int(dQ)\gamma_\omega^2(\tilde{\omega}_Q,Q),$$

$$\beta_1(\omega) = \eta\frac{\Delta}{\nu_0\Omega}\int(dQ)\gamma_\omega^2(\tilde{\omega}_Q,Q)(-i\tilde{\omega}_Q+DQ^2). \tag{3.32}$$

One can use Eq. (3.31) to present $\gamma_\omega(\zeta,Q)$ in the form

$$\gamma_\omega(\zeta,Q) = \frac{Z(\omega)}{-i\zeta+DQ^2+2m(\omega)}, \tag{3.33}$$

where the parameters $Z$ and $m$ are determined as

$$Z(\omega)=\frac{1}{f(\beta_0(\omega))},\qquad 2m(\omega)=\beta_1(\omega)\frac{f'(\beta_0(\omega))}{f(\beta_0(\omega))}. \tag{3.34}$$

It was already mentioned that the Hikami boxes $B^{(n)}$ and thus coefficients $C_n$ as well as the function $f(x)$ do not depend on the number of dimensions $d$. In contrast, the $\omega$ dependence of parameters $\beta_0$, $\beta_1$, and $m$ are different at different dimensions. Let us first consider the 0D case in order to determine $f(x)$ explicitly. At $d=0$ one has to abolish integration over $Q$ in Eq. (3.32) and substitute the inverse mean level spacing $\overline{\delta}^{-1}$ for $\nu_0$ and $2(\omega-E^*)$ for $\widetilde{\omega}_Q$. The vertex $\gamma$ can be determined straightforwardly

$$\gamma_\omega(\zeta)=\int\frac{d\epsilon_i}{2\pi}G_{i\downarrow}(\omega)G^{0*}_{i\uparrow}(\omega-E_Z-\zeta), \tag{3.35}$$

where 0D GF $G_{i\sigma}$ and $G^0_{i\sigma}$ are determined by Eq. (2.12) [Eq. (2.13) for $W_0$ should be multiplied by $\sqrt{\eta}$] and by Eq. (2.5), respectively. Substitution of Eqs. (2.12) and (2.5) into Eq. (3.35) gives after the integration over $\epsilon_i$

$$\gamma_\omega(\zeta)=\frac{1}{2}\left[F_0\left(\frac{\omega-E^*}{W_0}\right)+1\right]\times\frac{1}{-i\zeta+i(\omega-E^*)\{1-1/F_0[(\omega-E^*)/W_0]\}}, \tag{3.36}$$

where the function $F_0(x)$ is given by Eq. (2.15), $E^*$ is determined by Eq. (1.7), and $W_0^2=\eta\overline{\delta}\Delta^2/\Omega$. By comparing Eq. (3.36) with Eq. (3.33) we immediately obtain $Z(\omega)$ and $m(\omega)$ for zero dimensions:

$$Z_0(\omega)=\frac{F_0[(\omega-E^*)/W_0]+1}{2}, \tag{3.37}$$

$$m_0(\omega)=i(\omega-E^*)\frac{F_0[(\omega-E^*)/W_0]-1}{2F_0[(\omega-E^*)/W_0]}. \tag{3.38}$$

On the other hand, from the zero-dimensional version of Eq. (3.32) at $\zeta=2\omega-2E^*$ we can determine $\beta_0$ and $\beta_1$:

$$\beta_0=\frac{1}{4F_0^2},\quad \beta_1=-2i\omega=\frac{-i\omega}{F_0^2}. \tag{3.39}$$

Now we are in a position to determine the function $f(x)$ from Eq. (3.30). We express $F_0$ through $\beta_0$, substitute it into Eq. (3.37) for $Z_0$ and use the connection Eq. (3.34) between $Z_0(\omega)$ and $f(\beta_0)$. As a result we have

$$f(x)=\frac{1}{2x}-\frac{1}{F_0(2x)}=\frac{1}{2x}-\frac{\sqrt{1-4x}}{2x}. \tag{3.40}$$

This functional dependence which remains the same at all dimensions, can be used to evaluate $\delta\nu_\downarrow(\omega)$ for $d=1,2$.

Equations (3.23), (3.32)–(3.34), and (3.40) constitute a complete set allowing us to find the DOS in any dimension. One has to substitute Eq. (3.33) into Eq. (3.32), and find functions $Z(\omega)$ and $m(\omega)$ self-consistently with the help of Eqs. (3.34) and (3.40). The result should be substituted in Eq. (3.23) which gives the final nonperturbative answer for the DOS. In the following subsection, this program will be carried out for 1D (wires) and 2D (films) systems.

### *2. Solution of self-consistency equations*

We substitute Eq. (3.33) into Eqs. (3.32) and (3.23) and perform the integration over the wave vectors $Q$. Equation (3.23) acquires the form

$$\frac{\delta\nu_\sigma}{\nu_0}=-2\frac{\partial}{\partial\omega}\,\mathrm{Im}\int_0^1 d\eta\,\frac{M_d[-i\omega+m(\omega,\eta)]}{f[\beta_0(\omega,\eta)]}. \tag{3.41}$$

Here, we used Eq. (3.34) and introduced the dimensionless frequency and mass

$$\omega\to\frac{\omega+\sigma E^*}{W_d},\quad m\to\frac{m}{W_d}. \tag{3.42}$$

The relevant energy scales, which, as we will see below, are the widths of the tunneling anomaly, are given by

$$W_1=3\left(\frac{\Delta^2}{16\nu_1\Omega\sqrt{D}}\right)^{2/3},\quad W_2=\frac{\Delta^2}{4g\Omega}, \tag{3.43}$$

where $\Omega$ is given by Eq. (2.8), $D$ is the diffusion coefficient, $\nu_1=(mp_FS)/(2\pi^2)$ is the one-dimensional density of states per unit spin ($S$ is the cross section of the wire), and $g=4\pi\nu_2 D$ is the dimensionless conductance.[15] The latter is related to the normal-state resistance of the film as $g=25.8\mathrm{k}\Omega/R_\square$.

Dimensionless functions in Eq. (3.41), $M_d(x)$, are defined as

$$M_1(x)=\frac{2}{\sqrt{3x}},\quad M_2(x)=\ln\left(\frac{4g}{x}\right). \tag{3.44}$$

To find $M_2$ we cut off the logarithmic divergence at large momenta $Q$ by the condition $DQ^2\lesssim\Delta$, which determines the applicability of the single pole approximation (3.8), and neglected the factor $\Delta/\Omega\simeq 1$ in the argument of the logarithm.

Using the same notation, we obtain from Eqs. (3.32) and (3.34)

$$\beta_0(\omega,\eta)\{f[\beta_0(\omega,\eta)]\}^2=-\eta M_d'[-i\omega+m(\omega,\eta)], \tag{3.45a}$$

$$m\{f[\beta_0(\omega,\eta)]\}^3=\eta f'[\beta_0(\omega,\eta)]\{M_d[-i\omega+m(\omega,\eta)]+m(\omega,\eta)M_d'[-i\omega+m(\omega,\eta)]\}. \tag{3.45b}$$

Equation (3.40) allows us to formally solve Eq. (3.45a):

$$\beta_0=-\frac{\eta M_d'(-i\omega+m)}{[1-\eta M_d'(-i\omega+m)]^2}, \tag{3.46a}$$

$$f(\beta_0)=1-\eta M_d'(-i\omega+m), \tag{3.46b}$$

$$\frac{f'(\beta_0)}{[f(\beta_0)]^3}=\frac{1}{1+\eta M_d'(-i\omega+m)}. \tag{3.46c}$$

We can now substitute Eq. (3.46c) into Eq. (3.45b) and obtain after simple algebra

$$m(\omega,\eta)=\eta M_d[-i\omega+m(\omega,\eta)]. \tag{3.47}$$

The further calculations are substantially simplified due to the fact that the integrand in Eq. (3.41) can be presented as a total derivative with respect to $\eta$. In order to demonstrate this, we differentiate both sides of Eq. (3.47) with respect to $\eta$:

$$\frac{\partial m}{\partial \eta}=M_d(-i\omega+m)+\eta M_d'(-i\omega+m)\frac{\partial m}{\partial \eta}. \tag{3.48}$$

Finding $\partial m/\partial\eta$ from Eq. (3.48), we notice with the help of Eq. (3.46b) that it coincides with the integrand in Eq. (3.41). The integration in Eq. (3.41) can be immediately performed and we obtain

$$\frac{\delta\nu_\sigma}{\nu_0}=-2\frac{\partial}{\partial\omega}\,\mathrm{Im}\; m(\omega,\eta=1). \tag{3.49}$$

Finally we put $\eta=1$ in Eq. (3.47), differentiate both sides of this equation with respect to $\omega$, and substitute the result for $\partial m/\partial\omega$ into Eq. (3.49). After restoration of the original units for $\omega$ according to Eq. (3.42), we obtain for the density of states $\nu_\sigma(\omega)=\nu_0+\delta\nu_\sigma(\omega)$ the following result:

$$\frac{\nu_\sigma(\omega)}{\nu_0}=F_d\left(\frac{\omega+\sigma E^*}{W_d}\right), \tag{3.50}$$

where $\sigma=\pm1$ corresponds to the spin-up and spin-down densities of states, respectively, and the widths of the singularity $W_d$ are defined in Eq. (3.43). The dimensionless function $F_d(x)$ is given by

$$F_d(x)=\mathrm{Re}\frac{1+z(x)}{1-z(x)}, \tag{3.51a}$$

where the function $z(x)$ is implicitly defined as the solution of equations

$$z(x)=M_d'[-ix+y(x)],$$

$$y(x)=M_d[-ix+y(x)], \tag{3.51b}$$

with functions $M_d(x)$ being defined in Eq. (3.44). If Eq. (3.51b) has several solutions, one has to choose the one reproducing the perturbation theory at $x\gg1$ and remaining on the same sheet of the Riemann surface at small $x$.

In the 1D case, Eq. (3.51b) can be rewritten as a cubic equation and solved using the Cardano formula which yields a universal (independent of $\nu_1$ and $D$) expression for the shape of the singularity:

$$F_1(x)=1-\frac{2}{3}\,\mathrm{Re}\{1-ix[\sqrt[3]{1+y(x)}+\sqrt[3]{1-y(x)}]\}^{-1},$$

$$y(x)=\sqrt{1+ix^3}. \tag{3.52}$$

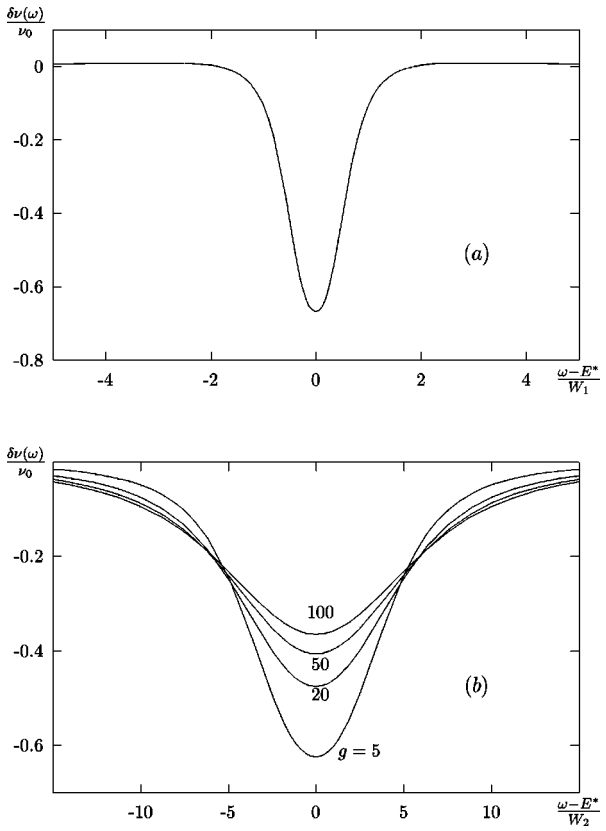


FIG. 13. Singularity in the DOS for spin-down polarized electrons for (a) 1D and (b) 2D systems. The widths of the singularity $W_{1,2}$ are given by Eq. (3.43), and the shape is defined by Eqs. (3.50), (3.52), and (3.53).

The functions $\sqrt[3]{z}$ in Eq. (3.52) are defined to the map complex plane $-\pi<\arg(z)<\pi$ to $-\pi/3<\arg(z)<\pi/3$.

For the two-dimensional case, we obtain from Eqs. (3.51) and (3.44):

$$F_2(x)=\mathrm{Re}\,\frac{1-z(x)}{1+z(x)}, \tag{3.53}$$

where $z(x)$ is the solution of the transcendental equation

$$z(x)=\frac{1}{-ix+\ln[4gz(x)]}. \tag{3.54}$$

The shape of the singularity in this case depends on the conductance $g$ and, thus, is not universal. However, this dependence is rather weak. For $|\omega\pm E^*|\gg W_d$, Eqs. (3.52) and (3.53) match the perturbative results, Eqs. (3.11) and (3.13). The found energy dependence of the density of states is shown in Fig. 13.

## IV. QUALITATIVE DISCUSSION

In this section we will present a simple qualitative interpretation of the main results obtained in the previous sections. We believe that this simplified way of thinking provides instructive physical intuition even though it fails to give a completely quantitative description.

It has been already emphasized in the beginning of section Sec. II that the ground state of the system above the paramagnetic limit has a structure similar to that of a nonin-

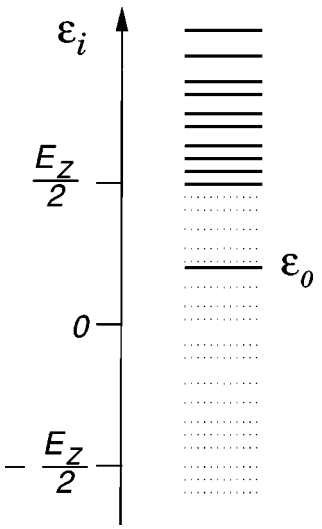


FIG. 14. Hilbert space for the solution of the two-electron problem. All the orbitals (dotted lines) with $\epsilon_i < -E_Z/2$ are excluded since they are occupied by ''frozen'' electron pairs and the orbitals $-E_Z/2 < \epsilon_i < E_Z/2$, $\epsilon_i \neq \epsilon_0$ are excluded because singly-occupied orbitals are not affected by the interaction (2.1).

teracting system. All the mixing of the noninteracting states caused by the interaction part of the Hamiltonian (2.1) is perturbative. We can neglect it completely in a rough approximation and consider the electrons occupying orbitals with orbital energies $\epsilon_i < -E_Z/2$, see Fig. 2, to be ''frozen.'' As soon as the spin down electron tunnels onto an orbital $0 < \epsilon_0 < E_Z/2$, see Fig. 2, the electron pair on this orbital is created. Due to the interaction, this pair can mix with all the empty states, $\epsilon_i > E_Z/2$. It is this mixing which gives rise to the singularity in the DOS. On the other hand, within the same approximation, all the electrons on the orbitals $\epsilon_i < -E_Z/2$ can still be considered as ''frozen.'' ( This approximation is similar in spirit to the well-known Cooper procedure[16].)

Thus, we arrive at the following recipe for the evaluation of the energy of a one-electron excitation. First we have to find the eigenenergies $E^j_{(2)}(\epsilon_0)$ of the two-electron problem within the Hilbert space consisting of the orbital $\epsilon_0$ and of all the orbitals $\epsilon_i > E_Z/2$, see Fig. 14. (This energy spectrum naturally depends on $\epsilon_0$ as parameter.) Then, the energies $E^j_{\downarrow}(\epsilon_0)$ of the one-particle excitation, corresponding to the introduction of an electron onto the orbital $\epsilon_0$ are

$$E^j_{\downarrow}(\epsilon_0) = E^j_{(2)}(\epsilon_0) - \left(\epsilon_0 - \frac{E_Z}{2}\right), \tag{4.1}$$

since the total energy of the electron which occupied this orbital before the tunneling event was $\epsilon_0 - E_Z/2$, while the state of the rest of the electrons did not change. Accordingly, the density of states for spin-down electrons is given by

$$\nu_{\downarrow}(\omega) \simeq \sum_{j,\epsilon_0} \delta[\omega - E^j_{\downarrow}(\epsilon_0)]. \tag{4.2}$$

Now, we have to find the spectrum of two-electron eigenenergies $E^j_{(2)}(\epsilon_0)$. Since the interaction in the Hamiltonian involves only the spin-singlet orbitals, the wave function of the electron pair $\psi$ can be labeled by one orbital index and it is governed by the Schrödinger equation:

$$E^j_{(2)}\psi_i = 2\epsilon_i\psi_i - \lambda\overline{\delta}\sum_j \psi_j . \tag{4.3}$$

The eigenenergies $E^j_{(2)}$ can be determined from the following equation:

$$\frac{\overline{\delta}}{2\epsilon_0 - E^j_{(2)}} + \sum_{\epsilon_i > E_Z/2} \frac{\overline{\delta}}{2\epsilon_i - E^j_{(2)}} = \frac{1}{\lambda}. \tag{4.4}$$

For low-lying eigenstates $E^j_{(2)} < E_Z$, one can substitute the summation in Eq. (4.4) by an integration. Given the high-energy cutoff $\omega_c$, it yields

$$\frac{2\overline{\delta}}{2\epsilon_0 - E^j_{(2)}} = \ln\left(1 + \frac{E_Z - E^j_{(2)} - \Delta_b}{\Delta_b}\right), \tag{4.5}$$

where $\Delta_b = \omega_c \exp(-2/\lambda)$ is the binding energy of the Cooper pair.

As we will see in a moment, $|2\epsilon_0 - E^j_{(2)}| \gg \overline{\delta}$, and, therefore, the logarithm in Eq. (4.5) should be also small and it can be expanded in the Taylor series, $\ln(1+x) \approx x$, $|x| \ll 1$. Equation (4.5) is immediately simplified to

$$\frac{2\overline{\delta}}{2\epsilon_0 - E^j_{(2)}} = \frac{E_Z - \Delta_b - E^j_{(2)}}{\Delta_b},$$

and we obtain the solution for the two relevant eigenenergies:

$$E^{\pm}_{(2)}(\epsilon_0) = \epsilon_0 + \frac{\Omega_b}{2} \pm \sqrt{\left(\frac{\Omega_b}{2} - \epsilon_0\right)^2 + 2\overline{\delta}\Delta_b}. \tag{4.6}$$

All the other two-electron states have energies larger than $E_Z$ and they are not important for us. In Eq. (4.6), the energy

$$\Omega_b = E_Z - \Delta_b \tag{4.7}$$

has the meaning of the energy of the bound state of the Cooper pair measured from the Fermi level. It plays the role of the energy $\Omega$ from Eq. (2.8) in the rigorous solution. We will return to the discussion of the discrepancy between Eqs. (4.7) and (2.8) later.

Substituting Eq. (4.6) into Eq. (4.1), we obtain the energy of one-particle excitations

$$E^{\pm}_{\downarrow}(\epsilon_0) = E^*_b \pm \sqrt{\left(\frac{\Omega_b}{2} - \epsilon_0\right)^2 + 2\overline{\delta}\Delta_b}, \tag{4.8}$$

where the position of the singularity

$$E^*_b = \frac{E_Z + \Omega_b}{2} \tag{4.9}$$

is similar to the energy $E^*$ in the exact Eq. (2.11) up to the substitution $\Omega \to \Omega_b$.

According to Eqs. (4.2) and Eq. (4.8), the density of states *vanishes* in the energy strip $|E - E^*_b| < (2\overline{\delta}\Delta_b)^{1/2}$—a hard gap in the DOS is formed, compared with the exact result, Eq. (2.15). The origin of this tunneling anomaly is the

avoided crossing of the two-electron state formed by the tunneling electron (energy $2\epsilon_0$) with the bound state of the Cooper pair (energy $\Omega_b$).

It is also noteworthy that if a spin-up electron tunnels into the grain, it never finds the pair for itself, and, therefore, no tunneling anomaly happens in this case. It means that the overall DOS does not vanish but rather shows the suppression by a factor of 2. However, for the spin-polarized electrons tunneling into the grain, we predict the complete suppression of the tunneling DOS.

The same arguments allow to justify the similar singularity, when a spin-up electron with energy $-E_Z/2<E<0$ tunnels out from the system, while the spin-down electrons tunneling from the system are not affected.

The qualitative consideration above grasps the correct physics, however it fails to describe the effect quantitatively, it predicts correctly neither the position nor the width of the gap. This is similar to the discrepancy between the binding energy $\Delta_b$ in the original Cooper procedure and the correct BCS gap $\Delta$: all the electrons below the Fermi energy were frozen. To remedy this drawback, one has to employ the parametrically exact procedure described in Secs. II and III.

Let us now discuss the results obtained for the disordered bulk systems, Sec. III. They can be briefly summarized as follows: (i) the singularity in the DOS persists; (ii) its position does not change; (iii) the energy scale of the singularity depends on both disorder and dimensionality, see Eq. (3.43).

In order to understand the physics behind the singularities in the bulk systems, let us recall the meaning of the zero-dimensional approximation. Strictly speaking, it implies that during the time $t_E \simeq \hbar/E$, (where $E$ is the energy scale relevant for the problem), a diffusively moving electron can visit all of the system. The characteristic time of this diffusion is $\simeq L^2/D$, ($L$ is the characteristic size of the system) which means that the zero-dimensional approximation is applicable provided that the energy scale $E$ does not exceed the Thouless energy $E_c=\hbar D/L^2$. In our problem the relevant energy scale is the gap width $W_0$ from Eq. (2.13), and the condition

$$1>\frac{W_0}{E_c}\propto L^{2-d/2} \tag{4.10}$$

is definitely violated for infinite systems $L\to\infty$, (here $d=1,2$ is the dimensionality of the system).

It is clear that as soon as the condition (4.10) breaks down the geometrical size of the system $L$ as well as its mean level spacing $\overline{\delta}=1/(\nu_0 L^d)$ is not relevant since the electron cannot diffuse during finite time $t_E=\hbar/E$ over a distance larger than $L_E=\sqrt{Dt_E}$. On the other hand, it effectively visits all the space on the scale smaller than $L_E$. Therefore, the following approximation holds: in order to understand the properties of the diffusive system associated with the energy scale $E$, we can separate the system into smaller patches of the size $L_E=\sqrt{\hbar D/E}$, and, then, apply the zero-dimensional description to each patch independently, (assuming that different patches do not ''talk'' to each other).

Let us now apply this strategy to the problem at hand. First, we notice that the position of the singularity in the 0D grain Eq. (2.11) does not depend on the size of the grain and therefore the singularity in each patch should be at the same energy $E^*$ as in zero-dimensional systems. Second, the level spacing $\overline{\delta}$ entering into the width of the singularity Eq. (2.13) does depend on the size of the patch

$$\overline{\delta}=\frac{1}{\nu_0 L_E^d}. \tag{4.11}$$

In this formula, scale $L_E$ is itself determined by the width of the singularity, $E\simeq W_d$, so that the scale $W_d$ has to be determined self-consistently. Substituting Eq. (4.11) into Eq. (2.13), we find

$$W_d\simeq\left(\frac{\Delta^2}{\nu_0 L_W^d\Omega}\right)^{1/2};\quad L_W\simeq\left(\frac{D}{W_d}\right)^{1/2}. \tag{4.12}$$

Solving Eq. (4.12), we obtain

$$W_d\simeq\Delta\left(\frac{\Delta^{d/2}}{\nu_0\Omega D^{d/2}}\right)^{2/(4-d)}, \tag{4.13}$$

which agrees with the rigorous results (3.43) for one- ($d=1$) and two- ($d=2$) dimensional systems. However, the quantitative description requires machinery like that used in Sec. III.

## V. RELEVANT PERTURBATIONS

### A. Spin-orbit scattering

In our previous consideration we assumed that electronic spin is a good quantum number, i.e., impurity scattering of electrons does not cause spin flips. There are two sources of spin relaxation of conduction electrons: localized spins (paramagnetic impurities) and spin-orbit (SO) scattering of electrons by nonmagnetic disorder. The latter is characterized by the scattering amplitude

$$iv_{so}([\boldsymbol{p}_f\times\boldsymbol{p}_i]\cdot\boldsymbol{\sigma})/p_F^2, \tag{5.1}$$

where $\boldsymbol{p}_f$ and $\boldsymbol{p}_i$ are final and initial momenta of an electron, and $\boldsymbol{\sigma}$ is the spin operator $\boldsymbol{\sigma}=(\hat{\sigma}_x,\hat{\sigma}_y,\hat{\sigma}_z)$ whose components are Pauli matrices. It acts on the spinor wave function of the electron.

Let us discuss the effect of SO scattering first starting with the qualitative physical picture. In the absence of both, SO interactions and magnetic field two-spin states, which belong to a given orbital, have the same energy. Magnetic fields split this degeneracy. It was important for us that the splitting $E_Z$ is exactly the same for all of the orbital states. Now let us turn to the SO interaction. Without an external magnetic field the states are still doubly degenerate due to $T$ invariance (Kramers doublets[17]). A magnetic field is well known to split the Kramers doublets similar to how it splits pure spin states in the absence of SO interactions. The main difference is that this splitting is not exactly uniform any more (see, e.g., Ref. 18). It is this dispersion of splittings that smears the DOS singularity. The Zeeman splitting dominates the magnetic-field effect on superconductivity only provided the SO interaction is weak. However the DOS singularity turns out to be sensitive even to a weak SO scattering, since the characteristic SO energy (the dispersion in the splitting of Kramers doublets) should be compared with the width of the

singularity $W_d$ rather than with the splitting $E_Z$ itself. The DOS for finite SO scattering can be evaluated in a way similar to our calculation in Sec. III B.

The Cooperon (or vertex) is formed by two electron Green functions. In the absence of external magnetic field it is convenient to classify Cooper poles by the total spin of two electrons $\boldsymbol{S}_+=(\boldsymbol{\sigma}_1+\boldsymbol{\sigma}_2)/2$. Spin-orbit scattering does not affect the spin singlet part of the Cooperon ($\boldsymbol{S}_+^2=0$) because the spin-orbit scattering preserves $T$ invariance. However, this scattering leads to total spin relaxation, i.e., the triplet ($\boldsymbol{S}_+^2=2$) component of the Cooperon decays (the pole in the $\omega$ plane is shifted from the real axis even for $Q=0$).[20]

An external magnetic field is coupled with the difference $\boldsymbol{S}_-=(\boldsymbol{\sigma}_1-\boldsymbol{\sigma}_2)/2$ of two electron spins, and as a result we classified the Cooperon by the eigenvalue of the operator $\boldsymbol{S}_-\cdot\boldsymbol{E}_Z$. These eigenvalues for $\boldsymbol{S}_-^2=2$ are $E_Z,0,-E_Z$ corresponding to $S_-^z=1,0,-1$ and 0 for $\boldsymbol{S}_-^2=0$. Neither of those two classifications is exact when both a magnetic field and SO scattering take place simultaneously: the operators $S_+^2$ and $S_-^z$ do not commute. On the other hand, as it was already mentioned, we should assume that the SO effect is weak. This allows us to evaluate the Cooperon perturbatively.

Summing the usual ladder diagrams and taking the additional scattering amplitude Eq. (5.1) into account, we end up with an equation for the $4\times4$ matrix of the Cooperon which we already discussed qualitatively:

$$\left[(-i\omega+DQ^2)\hat{I}+i\boldsymbol{E}_Z\cdot\boldsymbol{S}_-+\frac{2\boldsymbol{S}_+^2}{3\tau_{so}}\right]\hat{C}=\frac{\hat{I}}{\tau}, \tag{5.2}$$

where $\tau_{so}=1/(2\pi\nu_0 v_{so}^2)$ is the time of the spin relaxation by SO scattering, the matrix $\hat{I}$ is the direct product $\hat{I}=\sigma_0^s\otimes\sigma_0^e$, where the unit matrix $\sigma_0^s$ is acting in the spin $2\times2$ space, and $\sigma_0^e$ is the unit matrix in the $2\times2$ space of the electron lines. Operators $\boldsymbol{S}_\pm$ are defined as $2\boldsymbol{S}_+=(\boldsymbol{\sigma}^s+\boldsymbol{n}\sigma_0^s)\otimes\sigma_0^e$ and $2\boldsymbol{S}_-=(\boldsymbol{\sigma}^s-\boldsymbol{n}\sigma_0^s)\otimes\sigma_z^e$, where $\boldsymbol{n}=(1_x,1_y,1_z)$ is the unit vector, and $\boldsymbol{\sigma}^s=(\sigma_x^s,\sigma_y^s,\sigma_z^s)$ are the Pauli matrices in the spin space.

Instead of diagonalizing Eq. (5.2), we can just evaluate the correction to $C_{\uparrow(\downarrow)}^{-1}$,

$$C_\uparrow^{-1}\equiv[C^{-1}]_{\uparrow,\downarrow}^{\uparrow,\downarrow},\quad C_\downarrow^{-1}\equiv[C^{-1}]_{\downarrow,\uparrow}^{\downarrow,\uparrow} \tag{5.3}$$

in the first order of perturbation theory in $(E_Z\tau_{so})^{-1}\ll1$. This correction turns out to be $2/(3\tau_{so})$. As a result, SO scattering simply shifts the Cooper poles $C_{\uparrow(\downarrow)}$:

$$C_{\uparrow(\downarrow)}(\omega,Q)=\frac{1}{-i\omega\mp iE_Z+DQ^2+2/3\tau_{so}}. \tag{5.4}$$

From Eq. (5.4) one can guess that the all the interesting results can be obtained from the results of Secs. II and III by substituting

$$\omega\to\omega+i\Gamma, \tag{5.5}$$

where $\Gamma$ is the spin-orbit rate

$$\Gamma=\frac{2}{3\tau_{so}}, \tag{5.6}$$

so that the final result for the density of states is

$$\frac{\nu_{\uparrow(\downarrow)}(\omega)}{\nu_0}=\mathrm{Re}F_d\left(\frac{\omega\pm E^*+i\Gamma}{W_d}\right) \tag{5.7}$$

with $W_d$ and $E^*$ determined by Eqs. (2.13), (3.43), and (1.7), and dimensionless function $F_d$ is given by Eqs. (2.15), (3.52), and (3.53). We notice that the DOS singularity gets smeared by SO scattering when $\Gamma\gtrsim W_d$. This is in contrast to conventional superconductivity which is known to be stable with respect to SO scattering since the latter does not violate $T$ invariance.

This guess turns out to be correct. In order to demonstrate it one has to show that not only the Cooperon but also the Hikami boxes from Sec. III B are modified according to the rule (5.5). Taking into account the spin-orbit scattering Eq. (5.1) in impurity lines in Figs. 11 and 12, we obtain

$$B^{(2)}(\omega_1,\omega_2,Q_1,Q_2)=\frac{1}{(2\pi\nu_0)^3}\left[-i(\omega_1+\omega_2)+D(Q_1^2+Q_2^2)+\frac{4}{3\tau_{so}}\right],$$

$$B^{(3)}(\omega_1,\omega_2,\omega_3;Q_1,Q_2,Q_3)=-\frac{2}{(2\pi\nu_0)^5}[-i(\omega_1+\omega_2+\omega_3)+D(Q_1^2+Q_2^2+Q_3^2)+2\tau_{so}].$$

With the same rigor as in Sec. III B, we conjecture that

$$B^{(n)}\{\omega_j,Q_j\}=\frac{C_n}{(2\pi\nu_0)^{2n-1}}\sum_{j=1}^{n}\left(-i\omega_j+DQ_j^2+\frac{2}{3\tau_{so}}\right),$$

therefore, rule (5.5) is satisfied which gives Eq. (5.7).

Finally we emphasize that in Eq. (5.7) the complex argument of the function $F_d(z)$ should be located on the physical sheet: $z=|z|\exp i\varphi$ and $-\pi<\varphi<\pi$. Thus, the functions $\sqrt[d]{z}$ in Eqs. (2.15) and (3.52) are defined to map the complex plane $-\pi<\arg(z)<\pi$ to $-\pi/d<\arg(z)<\pi/d$.

### B. Paramagnetic impurities, orbital effects of the magnetic field

The derivation in the previous section suggests that any physical mechanism of violation of either $T$ invariance or conservation of spin will have a similar effect on the DOS singularity. Indeed, in the 0D and 1D cases in the presence of magnetic field $H$ and paramagnetic spins, Eq. (3.10) takes the following form:[4]

$$C(\omega,Q)=\frac{1}{-i\omega+DQ^2+1/\tau_{tot}}, \tag{5.8}$$

where $\tau_{tot}$ is a combination of phase and spin-relaxation effects

$$\frac{1}{\tau_{tot}}=\frac{1}{t_\varphi}+\frac{1}{t_s}. \tag{5.9}$$

Both SO scattering and spin exchange with paramagnetic impurities ($\tau_s$) lead to spin relaxation:

$$\frac{1}{t_s}=\frac{2}{3}\left(\frac{1}{\tau_{\rm so}}+\frac{1}{\tau_s}\right). \tag{5.10}$$

The phase may relax either due to inelastic processes or due to the magnetic field's effect on the orbital motion of the electrons:

$$\frac{1}{t_\varphi}=\frac{1}{\tau_\varphi}+\frac{1}{\tau_H}. \tag{5.11}$$

When the transverse dimension of the wire (size of the grain) $a$, exceeds the mean free path $l$, $\tau_H$ can be estimated as[4,22]

$$\frac{1}{\tau_H}=A\frac{\Omega_H^2}{E_T}\propto D\left(\frac{aH}{\phi_0}\right)^2. \tag{5.12}$$

Here $\phi_0=hc/2e\simeq 2\times 10^{-7}$ Gs cm$^2$ is the superconductivity magnetic flux, $E_T$ is the ''transverse'' Thouless energy, $E_T=D/a^2$, and $\Omega_H$ is the Cooperon ''cyclotron frequency'' (cyclotron frequency for a particle which mass and charge equal to $(2D)^{-1}$ and $2e$, respectively):[4]

$$\Omega_H=\frac{4DeH}{\hbar c}. \tag{5.13}$$

The numerical coefficient $A$ is not universal: it depends on the geometry of the superconductor, on the direction of magnetic field, etc.

Equations (5.8)–(5.13) are valid also for 2D films provided $H$ is parallel to the film plane. In this case

$$\frac{1}{\tau_H}=\frac{a^2\Omega_H^2}{48D}=\frac{D(eHa)^2}{3c^2\hbar^2}. \tag{5.14}$$

Now, we again conjecture that Eq. (3.28) for Hikami boxes is still valid with the addition of $1/\tau_{\rm tot}$ to all $DQ_j^2$. If so, Eq. (5.7) for DOS is still valid, but instead of Eq. (5.6) we should substitute

$$\Gamma=\frac{1}{\tau_{\rm tot}}. \tag{5.15}$$

The rate $\tau_\varphi^{-1}$ in Eq. (5.11) is the contribution of inelastic collisions. This contribution will be estimated in the next section. The evolution of the density of states with the rate $\alpha=\Gamma/W_d$ for different dimensions is shown in Fig. 15.

### C. Finite-temperature and inelastic processes

Our previous consideration, strictly speaking, applies only when the temperature $T$ equals zero. Let us now discuss the effects of finite $T$.

Temperature manifests itself through a distribution of electrons in energy. This distribution substantially depends on $T$ only for energies of the order of $T$. On the other hand, for tunneling anomalies at finite bias $eV\sim E^*$, Eq. (1.7), only the low-temperature region $T\ll E^*$ (recall that the Zeeman splitting $E_Z$ as well as superconducting gap $\Delta$ are normally of the order of $E^*$) is of interest. Indeed, thermal broadening

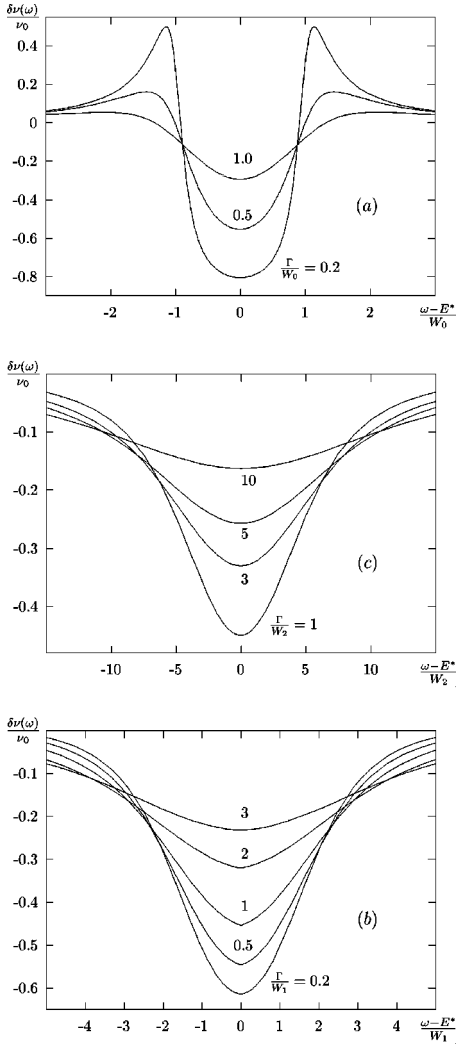


FIG. 15. Singularity in the DOS for spin-down polarized electrons for (a) 0D, (b) 1D, and (c) 2D systems for different values of the dimensionless rate $\alpha=\Gamma/W_d$. The DOS in the two-dimensional case is plotted for conductance $g=10$.

of the Fermi steps in the leads washes out any singularity as soon as $T$ exceeds the width $W$ of this singularity. Since the widths $W_d$, Eqs. (2.13) and (3.43), are much smaller than $E^*$, there will be already no anomaly of the tunneling current at $T\sim E^*$. On the other hand, at $T\ll E^*$ the equilibrium occupation number of a state with the energy of the order of $E^*$ is exponentially small and thus can be neglected. Therefore, formally determined DOS, Eq. (3.50) is temperature independent up to terms of the order of $\exp(-E^*/T)$. However, the observable, namely tunneling conductance $\sigma_T(eV)$, depends on $T$ through the Fermi distribution $n_F(\omega/T)$ in the leads. To evaluate the singular part $\delta\sigma_T(eV)$ of the tunneling conductance, one has to convolute $\delta\nu(\omega)$ with the derivative of the biased Fermi distribution:

$$\frac{\delta\sigma_T(eV)}{\sigma_T^0}=-\int d\omega\,\frac{\partial n_F[(\omega-eV)/T]}{\partial\omega}\,\frac{\delta\nu_\uparrow(\omega)+\delta\nu_\downarrow(\omega)}{\nu_0}. \tag{5.16}$$

Substitution of Eq. (3.50) into Eq. (5.16) yields for $\sigma_T=\sigma_T^0+\delta\sigma_T$:

$$\frac{\sigma_T(eV)}{\sigma_T^0}=\int \frac{d\omega}{4T\cosh^2[(\omega-eV)/2T]} \times \sum_{\sigma=\pm 1} \mathrm{Re}F_d\left(\frac{\omega+\sigma E^*+i\Gamma}{W_d}\right). \quad (5.17)$$

To complete this discussion, let us estimate the contribution of inelastic collisions of electrons, $1/\tau_\varphi$ Eq. (5.11), to $\Gamma$. Since we are dealing with rather highly excited states ($\omega \sim E^* \gg T$), the relaxation rate $1/\tau_\varphi$ is determined by large energy transfer ($\sim E^*$), and thus is temperature independent. In all interesting cases $1/\tau_\varphi$ simply coincides with the energy relaxation rate $1/\tau_\epsilon$. The latter (in metals, for reasonably low energies $\omega$) is determined by inelastic collisions between electrons (see Ref. 4 for a review) and can be estimated as

$$\frac{1}{\tau_\varphi}\simeq\frac{1}{\tau_\epsilon}\sim\frac{1}{\nu_0 L_\omega^d}=\frac{\omega}{g(L_\omega)}, \quad (5.18)$$

where $L_\omega=\sqrt{D/\omega}$ is the length of diffusion in time $\omega^{-1}$ and $g(L)=\nu_0 D L^{d-2}$ is the conductance of the $d$-dimensional sample with size $L$. For the zero-dimensional case inelastic processes of this type can be neglected completely since $1/\tau_\varphi$ compares with the level spacing only at energies $E^*$ of the order of the Thouless energy.[13,21]

Using Eqs. (4.13) we can estimate the dimensionless product $W_d\tau_\varphi$ as

$$W_d\tau_\varphi\sim\left(\frac{\Delta}{\Omega}\right)^{2/(4-d)} g(\xi)^{(2-d)/(4-d)} \sim\left(\frac{\Delta}{\Omega}\right)^{2/4-d}\times\begin{cases} g^{1/3}(\xi) & d=1 \\ \ln g(\xi) & d=2, \end{cases} \quad (5.19)$$

where $\xi=L_\Delta$ is the coherence length. Since $\Delta\sim\Omega$, this estimate implies that as long as the localization length $L_{\mathrm{loc}}$ exceeds $\xi$, the width $W_d$ is much bigger than $1/\tau_\varphi$ and inelastic collisions are irrelevant [$L_{\mathrm{loc}}$ can be estimated from the equation $g(L_{\mathrm{loc}})\sim 1$].

Together with Eqs. (2.13) and (3.43) for $W_d$ and Eqs. (5.9)–(5.15) for $\Gamma$, Eq. (5.17) completely describes the tunneling anomalies at $eV\sim\pm E^*$ for $W_d\gtrsim T,\Gamma$ and $d=0,1$. For $d=2$, Eq. (5.17) is valid only provided that the external magnetic field is parallel to the plane. The orbital effect of this perpendicular component on the tunneling anomaly is discussed in the next section.

### D. Magnetic field perpendicular to the film

It was already mentioned that for zero- and one-dimensional cases orbital effects of the magnetic field manifest themselves through the addition $1/\tau_H$ from Eq. (5.12), to the parameter $\Gamma$, see Eqs. (5.6), (5.13), and (5.15). The same is true in two dimensions provided the magnetic field is parallel to the film plane.[4] However, the effect of a component of the magnetic field perpendicular to the plane requires a separate consideration.

Similarly to the usual calculation of the anomalous magnetoresistance,[22,4] we need to derive and to solve the equation for the Cooperon in a perpendicular magnetic field rather than to take this field into account perturbatively. This equation is well known to be a Schrödinger equation in imaginary time for a particle with charge $2e$ and mass $1/(2D)$ in the magnetic field $H$. For $H=0$ the eigenfunctions of this equation are plane waves. When this field $H$ is finite but parallel to the plane and weak enough [magnetic length $l_H=(\hbar c/eH)^{1/2}$ exceeds the film thickness $a$, or $\Omega_H$ of Eq. (5.13) is smaller than the ''perpendicular'' Thouless energy $E_T=D/a^2$], it can be taken into account perturbatively. The eigenfunctions remain plane waves, so that Cooperon keeps its form Eq. (5.8), but the eigenvalues are shifted by $\tau_H^{-1}$.

In contrast, even a weak perpendicular component of $H$ changes the eigenfunctions, and as a result the form of the Cooper pole is also modified. Each eigenfunction should be characterized by the number of its Landau band $n$ and by one of the components of momentum $Q$ (one of the coordinates of the guiding center) rather than by both components of the momentum. The corresponding eigenvalue equals $\Omega_H(n+1/2)$, where $\Omega_H$ is given by Eq. (5.13), i.e., it is determined by the number of its Landau band, and it is independent of the location of the center.

As a result, in all previous calculations $DQ_j^2$ should be substituted by $\Omega_H(n+1/2)$, and instead of integrating over $(dQ_j)$, we have to sum over $n$ and divide the result by $4\pi l_H^2$. At $H=0$, the integration over $dQ$ is limited from above by $DQ^2\lesssim\Delta$, see the discussion after Eq. (3.44). For the same reason we sum over $n$ from 1 till $N\simeq\Delta/\Omega_H$. In order to evaluate $\delta\nu_\sigma(\omega)$, we have to perform a calculation similar to that of Sec. III with such changes.

Equation (3.23) for the DOS should be rewritten as

$$\frac{\delta\nu_\sigma(\omega)}{\nu_0}=-\frac{\Delta^2}{\nu_0\Omega}\,\mathrm{Im}\,\frac{\partial}{\partial\omega}\int_0^1 d\eta\,\frac{1}{4\pi l_H^2}\sum_{n=1}^{N}\gamma_\omega(\omega_{n\sigma},n), \quad (5.20)$$

where $\sigma=\pm 1$ corresponds to $\uparrow$ and $\downarrow$, respectively, and the short-hand notation

$$\omega_{n\sigma}=2(\omega+\sigma E^*)+i\Omega_H\left(n+\frac{1}{2}\right), \quad (5.21)$$

is introduced. After an obvious modification of Eq. (3.31), we obtain instead of Eq. (3.33)

$$\gamma_\omega(\zeta,n)=\frac{Z(\omega)}{-i\zeta+\Omega_H(n+1/2)+2m(\omega)}, \quad (5.22)$$

where $Z(\omega)$ and $m(\omega)$ can still be expressed through $\beta_0$ and $\beta_1$ according to Eq. (3.34). Consequently, the functions $\beta_0(\omega)$ and $\beta_1(\omega)$ can be connected with $\gamma_\omega(\zeta,n)$ by equations similar to Eq. (3.32):

$$\beta_p(\omega)=\eta\frac{\Delta}{\nu_0\Omega}\sum_{n=1}^{N}\frac{\gamma_\omega^2(\omega_n,n)}{[-i\omega_n+\Omega_H(n+1/2)]^p}. \quad (5.23)$$

Equation (5.23) is valid for $p=0,1$ and for both spin directions. We substitute Eq. (3.33) into Eqs. (5.20) and (5.23), carry out the summation over $n$, and obtain Eqs. (3.41) and (3.43). The scale of the singularity coincides with $W_2$ from Eq. (3.43), while the dimensionless function $M_d$ is replaced with

$$M_H(x)=\ln\left(\frac{\Delta}{\Omega_H}\right)-\psi\left(\frac{1}{2}+\frac{x}{\alpha_H}\right). \tag{5.24}$$

Here, the orbital effect of the magnetic field is characterized by dimensionless parameter $\alpha_H=\Omega_H/W_2$ and $\psi(x)$ is the digamma function

$$\psi(x)=\sum_{n=0}^{\infty}\left(\frac{1}{n+1}-\frac{1}{n+x}\right)-\boldsymbol{C},$$

and $\boldsymbol{C}\approx 0.577\ldots$ is the Euler constant. If the magnetic field is weak $\alpha_H \ll 1$, we can use the asymptotic expansion $\psi(x) \approx \ln x$, $x \gg 1$ and recover the two-dimensional result $M_2$ from Eq. (3.44). Since the function $M_H$ depends on the additional variable $\alpha_H$ only, on a parameter we can use the solution of Sec. III B to obtain the density of states:

$$\frac{\nu_\sigma(\omega)}{\nu_0}=F_H\left(\frac{\omega-\sigma E^*+i\Gamma}{W_2}\right), \tag{5.25}$$

where the energy scale $W_2$ is given by Eq. (3.43), we included previously discussed broadening mechanisms according to rule (5.5) with the rate $\Gamma$ given by Eq. (5.15). The dimensionless function $F_H(x)$ is given by

$$F_H(x)=\mathrm{Re}\frac{\alpha_H-\psi'\{1/2+[-ix+y(x)]/\alpha_H\}}{\alpha_H+\psi'[1/2+[-ix+y(x)]/\alpha_H\}}, \tag{5.26}$$

where the function $y(x)$ is the solution of the equation

$$y(x)=\ln 4g-\ln\alpha_H-\psi\left(\frac{1}{2}+\frac{-ix+y(x)}{\alpha_H}\right).$$

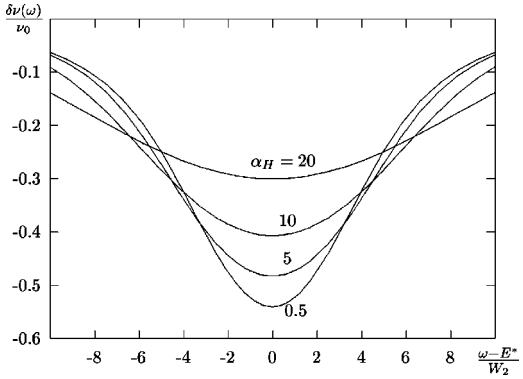


FIG. 16. The singularity in the DOS of two-dimensional films for spin-down polarized electrons for different values of the dimensionless magnetic field $\alpha_H=\Omega_H/W_2$. The curves are plotted for a conductance of $g=10$.

The density of states in two-dimensional films for different values of the parameter $\alpha_H$ is shown in Fig. 16.

Closing this subsection, we present the asymptotic behavior of $F_H(x)$ for two limiting cases. In weak fields $\alpha_H \ll 1$ the magnetic field slightly perturbs the two-dimensional result (3.53):

$$F_H(x)=F_2(x)+\frac{1}{12}\left(\frac{\Omega_H}{W_2}\right)^2\mathrm{Re}\frac{z^3(x)}{[1+z(x)]^2}, \tag{5.27}$$

where the dimensionless functions $F_2(x)$ and $z(x)$ are defined in Eqs. (3.53) and (3.54), respectively.

In the opposite limit $\alpha_H \gg \max(1,\Gamma/W_2)$ the depth of the singularity is controlled solely by the cyclotron frequency (5.13)

$$\frac{\nu_\sigma(\omega)}{\nu_0}=1-\begin{cases}\dfrac{W_2}{\Omega_H}\dfrac{\pi^2}{\cosh^2[(\omega+\sigma E^*)/\Omega_H]}, & |\omega+\sigma E^*|\lesssim\Omega_H;\\ 4\pi^2\dfrac{W_2}{\Omega_H}\exp\left(-2\dfrac{\omega+\sigma E^*}{\Omega_H}\right)+\left(\dfrac{W_2}{\omega+\sigma E^*}\right)^2\ln\left(\dfrac{\Omega}{\omega+\sigma E^*}\right)^2, & |\omega+\sigma E^*|\gg\Omega_H.\end{cases} \tag{5.28}$$

## VI. EXPERIMENTS ON Al FILMS

The theoretical study presented in this paper was inspired by the experimental work of Wu, Williams, and Adams.[8] These authors studied tunneling anomalies in ultrathin (about 4 nm thick) Al films, which were driven into the paramagnetic state by a parallel magnetic field $H>H_\parallel\simeq 4.8$ T. Both a zero-bias anomaly and anomalies at biases close to the Zeeman splitting $E_Z$ were observed. The authors attempted to fit the experimental results by the theory of Ref. 4, developed for normal metals and superconductors at $T>T_c$. The agreement appeared to be reasonable with one important exception: the positions of the satellite singularities $E^{**}$ were lower in energies than that predicted by Ref. 4: experimentally it was fitted as

$$E^{**}\simeq E_Z-E_0;\quad E_0=0.17\ \text{meV}. \tag{6.1}$$

In our theory $eV_s=E^*<E_Z$, see Eq. (1.7), and the discrepancy is reduced even though it does not disappear. For instance, the minimal value of $E^*$ corresponds to the phase-transition point $E_Z=\sqrt{2}\Delta$ and, according to Eq. (1.7), equals $\Delta(\sqrt{2}+1)/2\simeq 0.47$ meV, since $\Delta\simeq 0.39$ meV. The experimental value $eV_s\simeq 0.38$ meV is about 20% smaller (rather than 33% in comparison with Ref. 4). We do not have enough data to speculate about possible sources of this discrepancy. More experiments with serious quantitative analysis are needed to verify the present theory. Nevertheless, it may be worthwhile to briefly discuss here how the other experimental findings of Ref. 8 compare with the theoretical conclusions.

In Ref. 8, the authors presented and discussed the tunneling conductance $G(V,H)$ as a function of bias voltage and

magnetic field for two samples. Both samples were granular Al films about 4 nm thick. Their sheet resistances were different: $R_{\square}^{(1)} \simeq 4.2\ \text{k}\Omega$, $R_{\square}^{(2)} \simeq 2.0\ \text{k}\Omega$. For both samples dips of the tunneling conductance at $V = \pm V_s$ were observed. The widths at half minimum (WHM) of these dips for both samples were about 0.15–0.2 meV, while the depths were found to be quite different: $|\delta G/G|^{(1)} \simeq 0.12$ and $|\delta G/G|^{(2)} \simeq 0.05$.

One can interpret these experimental results in two different ways. The first interpretation is based on the assumption that the granular structure of the films is irrelevant, and they can be approximated as homogeneous 2D objects. Given the superconducting gap $\Delta \simeq 0.39$ meV, Zeeman splitting $E_Z \simeq 0.57$ meV at magnetic field $H = 5$ T, and $R_{\square}$, one can use Eq. (3.43) to determine $W_2$: $W_2^{(1)} \simeq 0.03$ meV; $W_2^{(2)} \simeq 0.015$ meV. Since the WHM of the anomaly should be compared with approximately $2W_2$, see Fig. 15(c), we have not great but reasonable agreement, especially for the first sample. However the law $W_2 \propto \ln(g)/g$ from Eqs. (3.43) and (3.53) seems to contradict the experiment.

The alternative interpretation is based on the approximation of weakly connected Al grains: in the first approximation we neglect the coupling between the grains. This allows us to use the 0D expression for the width of the singularity $W_0$, see Eq. (2.13). Given the electron concentration in Al of $n = 1.8 \times 10^{23}\ \text{cm}^{-3}$ and their Fermi energy $E_F = 11.8$ eV,[19] the bare DOS is estimated as $\nu \simeq 2 \times 10^{22}\ (\text{eV cm}^3)^{-1}$. Assuming that the grains in lateral directions have a typical size $b \simeq 30$ nm,[8] and that the film thickness is $a \simeq 4$ nm, we can estimate the mean level spacing $\overline{\delta} \simeq 1/(ab^2\nu) \simeq 0.03$ meV. Substitution of this value of $\overline{\delta}$ into Eq. (2.13) gives $W_0 \simeq 0.11$ meV. This is in a good agreement with the experiment, since the WHM at zero dimensions according to Fig. 15(a) should be compared with $2W_0 \simeq 0.22$.

In order to understand the substantial difference in amplitudes of the tunneling anomalies for the two samples, let us discuss the effect of coupling between the grains. This coupling results in a finite dwell time $\tau_{\text{dwell}}$ which an electron spends in a given grain before tunneling into a neighboring one. We can determine $\tau_{\text{dwell}}$ from $D$, the constant of the diffusion at times bigger than $\tau_{\text{dwell}}$, using the relation $D \simeq b^2/(2\tau_{\text{dwell}})$. Given the sheet resistance $R_{\square}^{(1,2)}$, DOS $\nu$, and the film thickness $a$, one can estimate $D$ as $D^{(1)} \simeq 0.2\ \text{cm}^2/\text{sec}$, $D^{(2)} \simeq 0.4\ \text{cm}^2/\text{sec}$. As a result

$$\frac{\hbar}{\tau_{\text{dwell}}^{(1)}} \simeq 0.05\ \text{meV}, \qquad \frac{\hbar}{\tau_{\text{dwell}}^{(2)}} \simeq 0.1\ \text{meV}.$$

Now we can explain the difference in the depths of the anomalies in the two samples assuming that $\hbar/\tau_d$ contributes to $\Gamma$ from Eq. (5.15). One can see from Fig. 15a that the dip at $\Gamma = W_0/2$ is approximately twice as deep as the one at $\Gamma = W_0$. At the same time, WHM's in these two cases are close to each other.

Note that Eq. (5.7) with $\Gamma = \hbar/\tau_{\text{dwell}}$ can be justified only for $\tau_{\text{dwell}} W_d > \hbar$. Theoretical investigation of the crossover between 0D and 2D behavior in granular films goes beyond the framework of this paper, though such a study can be important for a quantitative discussion of experiments.

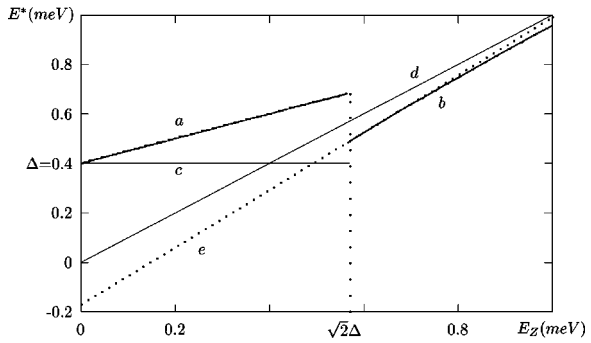


FIG. 17. Position of the minimum in the DOS as the function of the Zeeman splitting $E_Z$ for $\Delta \simeq 0.4$ meV: (a) Theoretical prediction for the superconducting state (Ref. 5), see Fig. 1(a); (b) Our theoretical prediction, Eq. (1.7) for the paramagnetic state; (c) Half distance between maxima in the DOS in the superconducting state: (d) $E^* = E_Z$ law predicted for the normal metal (Ref. 4); (e) Approximation of Eq. (1.7) by a straight line.

From the perpendicular critical field $H_{c\perp} \simeq 1.5$ T and the dimensions of a grain one can estimate $1/\tau_H$ and find that it is irrelevant for the experiment.[8] The same is correct for spin-orbit scattering. Recent studies of tunneling through Al grains[9] show that the difference of the $g$ factor from 2 is very small not only in average, but also for a given orbital as well. Both $\hbar/\tau_H$ and $\hbar/\tau_{\text{so}}$ are probably smaller than 0.01 meV and much smaller than $\hbar/\tau_{\text{dwell}}$.

Let us now return to the discussion of the dip location. Note that a dip in the DOS at the finite bias exists in both the superconducting and paramagnetic states. According to the idealized Fig. 1(a), on the superconducting side of the Clogston-Chandrasekhar phase transition, this anomaly is located at $eV = \Delta + E_Z/2$ (line ''a'' in Fig. 17). However, probably due to the smearing of the DOS singularities, experimentally the minimum was found in the middle between two peaks in the DOS, i.e., at $eV \simeq \Delta$ (line ''c'' in Fig. 17). As it was already mentioned, the experimentally found position of the singularity is lower than our theoretical prediction (1.7). In fact, no jump in $E^*$ was observed at the point of the first-order phase transition. This discrepancy may be due to the inhomogeneous broadening of the transition—different granulars may have slightly different $\Delta$. Another possibility is illustrated in Fig. 17. In the interval of magnetic fields where the measurements were done the theoretical dependence Eq. (1.7) (line ''b'' in Fig. 17) can be approximated by

$$E^* \approx rE_Z - 0.17\ \text{meV} \tag{6.2}$$

with a numerical factor $r \simeq 1.15$ slightly larger than 1 (line ''e'' in Fig. 17). Comparing Eq. (6.2) with the experimental fit (6.1), we see that the theory would agree with experiment very well if we assume that the actual $g$ factor is smaller than its bare value, i.e., $g_L = 2/r \approx 1.72$.

## VII. CONCLUSION

This paper is devoted to the anomalies of the tunneling density of states of low dimensional ($d = 0,1,2$) superconductors in an external magnetic field. We concentrated on the Clogston-Chandrasekhar (CC) phase transition, i.e., the destruction of superconductivity by a magnetic field by virtue

of the Zeeman splitting. As a result a normal paramagnetic state of electrons is formed.

The main conclusion we can draw from our study of the CC state is, that despite this state being normal (the mean-field superconducting order parameter vanishes), it is drastically different from a usual normal metal with some attractive interaction. The latter state appears, e.g., in a superconductor at temperatures higher than the transition temperature $T_c$. The difference becomes apparent when one studies excited states rather than those close to the ground state.

Superconducting fluctuations in a usual normal disordered metal were known to contribute to the zero-bias tunneling anomaly as well as to Zeeman anomalies at a bias $eV$ equal to Zeeman splitting.[4] However, these contributions [effects of the interaction in the Cooper channel] are similar or weaker than the effects of the Coulomb repulsion of electrons, unless the system is anomalously close to the transition, i.e., it is not in the Levanyuk-Ginzburg region. This means that the effects of superconducting fluctuations can be taken into account perturbatively almost everywhere, (except in the very vicinity of the transition temperature) if the system is not too dirty. The perturbative approach (expansion in inverse powers of the conductance $g$) is valid as long as all of the characteristic length scales involved in the problem do not exceed the localization length $L_{\rm loc}$.

The tunneling anomalies in the CC normal state studied by us are quite different. First of all, its position $eV=E^*$, see Eq. (1.7), is different from the Zeeman splitting $E_Z$. However, what is more important, the perturbative corrections to the density of states $\nu(\omega)$ are much more singular at $\omega$ close to $E^*$ than corrections of the same order in $g^{-1}$ in usual normal metals. Because of this, the perturbative approach fails in a parametrically wider energy interval $|eV-E^*| \leqslant W_d$ around the singular bias than that for the normal metal. Using Eqs. (3.43), one can check that the length scale $L_W$ which corresponds to $W_d$ is much less than $L_{\rm loc}^{(d)}$, provided $L_{\rm loc}$ exceeds the superconducting coherence length $\xi$. Indeed, since the localization length can be estimated as $L_{\rm loc}^{(1)} \simeq D\nu^{(1)}$ and $L_{\rm loc}^{(2)} \simeq l\exp(D\nu^{(2)})$, (where $l$ is the mean free path, $D$ is the diffusion coefficient, and $\nu^{(d)}$ is the $d$-dimensional DOS) the characteristic spatial scale corresponding to the singularity, $L_{W_d}$, can be written as

$$\frac{L_{W_1}}{L_{\rm loc}^{(1)}} \simeq \left(\frac{\xi}{L_{\rm loc}^{(1)}}\right)^{2/3},$$

$$\frac{L_{W_2}}{L_{\rm loc}^{(2)}} \simeq \frac{\xi}{L_{\rm loc}^{(2)}}\sqrt{\ln\left(\frac{L_{\rm loc}}{l}\right)}.$$

The fact that $W_d \gg D/L_{\rm loc}^2$ makes it necessary and also possible to go beyond perturbation theory—one has to sum only the most diverging terms, and one may neglect the usual weak localization and interaction corrections. It turns out to be possible to sum directly a whole series of the perturbation theory and thus determine the shapes of the singularities in all dimensions.

The singularities are characterized by their widths $W_d$ given by Eqs. (2.13) and (3.43). For zero-dimensional grains our theory predicts a hard gap in the density of states with a given spin direction, centered at $\omega=E^*$. For one-dimensional wires the shape becomes universal (independent on $\nu^{(1)}$ and $D$) when energy is measured in units of $W_1$, see Eq. (3.52). It means that the depth of the anomaly is universal. In the case of the two-dimensional film the depth of the anomaly is not universal and behaves as the inverse logarithm of the conductance, see Eq. (3.53).

The reason why the effects of superconducting fluctuations in a CC metal are dramatically enhanced in comparison with the usual case is the presence of the polelike singularity in the correlation function of these fluctuations. This pole at a finite frequency appears due to the fact that the CC transition is of the first order. In contrast, the temperature-driven transition from superconductor to normal metal is of the second order, and in a usual normal state the correlator of the superconducting fluctuations is a smooth function of the frequency, i.e., any superconducting excitations decay very rapidly. We believe that the strong anomalies of the excitation spectrum at finite energies is a generic feature of any state created as a result of a first-order quantum phase transition.

## ACKNOWLEDGMENTS

Discussions with A. I. Larkin and B. Z. Spivak are acknowledged with gratitude. We are grateful to J. von Delft for reading the manuscript.

[1] M. Tinkham, *Introduction to Superconductivity* (McGraw-Hill, New York, 1980).
[2] A. M. Clogston, Phys. Rev. Lett. **9**, 266 (1962); B. S. Chandrasekhar, Appl. Phys. Lett. **1**, 7 (1962).
[3] I. Giaever, Phys. Rev. Lett. **5**, 464 (1960).
[4] B. L. Altshuler and A. G. Aronov, in *Electron-Electron Interaction in Disordered Systems*, edited by A. L. Efros and M. Pollak (North-Holland, Amsterdam, 1985).
[5] P. Fulde, Adv. Phys. **22**, 667 (1973).
[6] I. L. Aleiner and B. L. Altshuler, Phys. Rev. Lett. **79**, 4242 (1997).
[7] A. A. Abrikosov, L. P. Gorkov, and I. E. Dzyaloshinskii, *Methods of Quantum Field Theory in Statistical Physics* (Prentice-Hall, Englewood Cliffs, NJ, 1963).
[8] W. Wu, J. Williams, and P. W. Adams, Phys. Rev. Lett. **77**, 1139 (1996).
[9] C. T. Black, D. C. Ralph, and M. Tinkham, Phys. Rev. Lett. **76**, 688 (1996).
[10] F. Braun, J. von Delft, D. C. Ralph, and M. Tinkham, Phys. Rev. Lett. **79**, 921 (1997).
[11] For review, see e.g., D. V. Averin and K. K. Likharev, in *Mesoscopic Phenomena in Solids*, edited by B. L. Altshuler, P. A. Lee, and R. A. Webb (North-Holland, New York, 1991).
[12] Ya. M. Blanter, Phys. Rev. B **54**, 12 807 (1996); O. Agam, N. S. Wingreen, B. L. Altshuler, D. C. Ralph, and M. Tinkham, Phys. Rev. Lett. **78**, 1956 (1997); Ya. M. Blanter and A. D. Mirlin, Phys. Rev. E **55**, 6514 (1997).

[13] B L. Altshuler, Y. Gefen, A. Kamenev, and L. S. Levitov, Phys. Rev. Lett. **78**, 2803 (1997).
[14] S. Hikami, Phys. Rev. B **24**, 2671 (1981).
[15] The numerical coefficient in the formula for $W_1$ is different from that in Ref. 6 because of the algebraic error in this reference.
[16] L. N. Cooper, Phys. Rev. **104**, 1189 (1956).
[17] H. A. Kramers, Proc. R. Acad. Sci. Amsterdam **33**, 959 (1930).
[18] V. E. Kravtsov and M. R. Zirnbauer, Phys. Rev. B **46**, 4332 (1992).
[19] N. W. Ashcroft and N. D Mermin, *Solid State Physics* (Holt, Rinehart, and Winston, New York, 1976).
[20] S. Hikami, A. I. Larkin, and Y. Nagaoka, Prog. Theor. Phys. **63**, 707 (1980).
[21] U. Sivan, Y. Imry, and A. Aronov, Europhys. Lett. **28**, 115 (1994).
[22] P. A. Lee and T. V. Ramakrishnan, Rev. Mod. Phys. **57**, 287 (1985).